BIOCHEMISTRY
including biophysical chemistry & molecular biology
Article

Biochemistry **2010,** *49,* 5117–5133 5117
DOI: 10.1021/bi100041f

Intermolecular Interactions in a 44 kDa Interferon−Receptor Complex Detected by Asymmetric Reverse-Protonation and Two-Dimensional NOESY†

Ilona Nudelman,[‡] Sabine R. Akabayov,[‡,||] Einat Schnur,[‡] Zohar Biron,[‡] Rina Levy,[‡] Yingqi Xu,[§,⊥] Daiwen Yang,[§] and Jacob Anglister*[,‡]

[‡]*Department of Structural Biology, Weizmann Institute of Science, Rehovot 76100, Israel, and* [§]*Department of Biological Sciences, National University of Singapore, 14 Science Drive 4, Singapore 117543* [||]*Present address: Department of Biological Chemistry and Molecular Pharmacology, Harvard Medical School, Boston, MA 02115.* [⊥]*Present address: Molecular Biosciences, Imperial College London, Exhibition Road, London SW7 2AZ, U.K.*

Received January 12, 2010; Revised Manuscript Received May 24, 2010

ABSTRACT: Type I interferons (IFNs) make up a family of homologous helical cytokines initiating strong antiviral and antiproliferative activity. All type I IFNs bind to a common cell surface receptor consisting of two subunits, IFNAR1 and IFNAR2, associating upon binding of interferon. We studied intermolecular interactions between IFNAR2-EC and IFNα2 using asymmetric reverse-protonation of the different complex components and two-dimensional homonuclear NOESY. This new approach revealed with an excellent signal-to-noise ratio 24 new intermolecular NOEs between the two molecules despite the low concentration of the complex (0.25 mM) and its high molecular mass (44 kDa). Sequential and side chain assignment of IFNAR2-EC and IFNα2 in their binary complex helped assign the intermolecular NOEs to the corresponding protons. A docking model of the IFNAR2-EC−IFNα2 complex was calculated on the basis of the intermolecular interactions found in this study as well as four double mutant cycle constraints, previously observed NOEs between a single pair of residues and the NMR mapping of the binding sites on IFNAR2-EC and IFNα2. Our docking model doubles the buried surface area of the previous model and significantly increases the number of intermolecular hydrogen bonds, salt bridges, and van der Waals interactions. Furthermore, our model reveals the participation of several new regions in the binding site such as the N-terminus and A helix of IFNα2 and the C domain of IFNAR2-EC. As a result of these additions, the orientation of IFNAR2-EC relative to IFNα2 has changed by 30° in comparison with a previously calculated model that was based on NMR mapping of the binding sites and double mutant cycle constraints. In addition, the new model strongly supports the recently proposed allosteric changes in IFNα2 upon binding of IFNAR1-EC to the binary IFNα2−IFNAR2-EC complex.

Type I IFNs[1] are a major component of the innate immune system protecting against viral infection. They provide an early line of defense, hours to days ahead of the adaptive immune response, and are essential for the survival of higher vertebrates (*1*−*3*). In addition to a strong antiviral activity, type I IFNs are also assigned antiproliferative and immunomodulatory properties (*4*, *5*).

All human type I IFNs elicit their activity through the same cell surface receptor consisting of two transmembrane protein subunits, IFNAR1 and IFNAR2 (*6*, *7*). IFNAR2 is the major ligand binding component and has nanomolar affinity for IFNs in the absence of IFNAR1. The affinity of the IFNAR1 subunit for IFNs is much lower, and the dissociation constant is in the micromolar range (*8*). The IFN signaling process begins with IFN-driven dimerization of the receptor subunits which initiates a tyrosine phosphorylation cascade inside the cell, resulting in transcription stimulation of genes responsible for the antiviral and antiproliferative response (*9*−*14*).

The three-dimensional structures of several IFNs, namely, human IFNα2a (*15*), IFNα2b (*16*), and IFNβ (*17*), have been determined. The structure of the 25 kDa extracellular domain of IFNAR2 was determined by our group using multidimensional NMR techniques (*18*). Mutagenesis, immunoblocking, and various NMR techniques were used to obtain information about residues in IFNα2 and IFNAR2-EC (hereafter termed IFNAR2) which participate in binding (*19*−*23*). The binding site on IFNAR2 was mapped to three loops in the N domain and the hinge region of the receptor. The binding site on IFNα2 was mapped to the A and E helices as well as the A−B loop. The binding affinity of the IFNα2−IFNAR2 complex is approximately 1 nM (*24*).

†This study was supported by the Israel Science Foundation, National Institutes of Health Grant GM53329, and the Kimmelman Center. J.A. is the Dr. Joseph and Ruth Owades Professor of Chemistry.

*To whom correspondence should be addressed. E-mail: Jacob.Anglister@weizmann.ac.il. Phone: 972-8-9343394. Fax: 972-8-9344136.

[1]Abbreviations: 2D, 3D, and 4D, two-, three-, and four-dimensional, respectively; AIR, ambiguous interaction restraints; CNS, Crystallography & NMR System; CT, constant time; D_2O, deuterium oxide; DMC, double mutant cycle; HCRII, class II helical cytokine receptor family; HSQC, heteronuclear single-quantum coherence; IFN, interferon; IFNAR1, first subunit of the receptor for class 1 interferons; IFNAR2, second subunit of the receptor for class 1 interferons; IFNAR2-EC, extracellular part of IFNAR2; INEPT, insensitive nuclei enhanced by polarization transfer; MBP, maltose binding protein; MQ, multiple quantum; MW, molecular weight; NMR, nuclear magnetic resonance; NOE, nuclear Overhauser enhancement; NOESY, nuclear Overhauser enhancement spectroscopy; PDB, Protein Data Bank; ^{R2}X and $^{\alpha 2}$Y, IFNAR2-EC and IFNα2 residues labeled with superscripts R2 and α2, respectively; RDC, residual dipolar coupling; rmsd, root-mean-square deviation; S/N, signal-to-noise ratio; TOCSY, total correlation spectroscopy; TROSY, transverse relaxation-optimized spectroscopy.

Published on Web 05/24/2010

Several models of the IFNAR2−IFNα2 complex have been computed recently. Roisman et al. calculated a docking model of IFNα2 with the modeled structure of IFNAR2-EC using site-directed mutagenesis mapping of the binding sites as well as five double mutant cycle (DMC) distance constraints (*25*). When the NMR structure of IFNAR2 had become available, Chill et al. calculated another docking model based on the four most significant of the five previously identified DMC constraints (*18*). The fifth DMC interaction, between ^{R2}Y43 on IFNAR2 and $^{\alpha 2}$F27 on IFNα2, was omitted from the calculation because it was incompatible with the IFNAR2 NMR structure (*18*). The latest docking model of the IFNAR2−IFNα2 complex was derived by Quadt-Akabayov et al. on the basis of the NMR mapping of the binding sites on IFNAR2 and IFNα2, four DMC constraints, and a single intermolecular NOE (*26*). The DMC data provided qualitative information about interactions that could be translated to distance constraints only very roughly. The DMC constraints, together with the observed NOEs between a single pair of residues and the NMR mapping of the binding sites, are not sufficient to define accurately the orientation of the two molecules in the complex.

In this study, we conducted high-resolution NMR investigations of the IFNAR2−IFNα2 complex to detect a larger number of intermolecular NOE interactions to better define the structure of the IFNAR2−IFNα2 complex. Acquiring such information about the 44 kDa IFNAR2−IFNα2 complex by NMR has presented considerable challenges because of its size and the conditions under which it is stable.

The size of biomolecules studied by NMR is limited by the enhanced transverse relaxation of carbon and hydrogen nuclei and increasing spectral complexity. In the past 10−15 years, several techniques have been introduced to help overcome these limitations. ^{13}C and ^{15}N labeling, higher-dimension spectra (*27*) as well as uniform deuteration of nonexchangeable protons (*28*, *29*), and TROSY-based triple-resonance experiments (*30*) have enabled sequential assignment of backbone nuclei of large proteins and macromolecular complexes. Backbone (HN, Cα, and C*β*) resonance assignment of uniformly ^{2}H-, ^{13}C-, and ^{15}N-labeled proteins up to a molecular mass of 100 kDa has been achieved (*31*, *32*). However, uniform deuteration of nonlabile protons, while vastly contributing to the increased signal-to-noise ratio in NMR spectra, eliminates all the proton probes giving rise to NOE interactions, except for the labile amide protons. Reverse-protonation of uniformly deuterated proteins has been applied to recapture distance information in high-molecular mass systems (*32*−*34*). Several approaches have been used to selectively reverse-label protons in proteins. One way is to supplement the D_2O-based bacterial growth medium with the desired ^{1}H-labeled, ^{1}H- and ^{15}N-labeled, or ^{1}H-, ^{15}N-, and ^{13}C-labeled amino acids. Reverse-protonation of a combination of aliphatic and aromatic residues such as ILVFY has been used in several NMR studies of large proteins and protein complexes to detect intramolecular aromatic−methyl NOEs instrumental to determination of their structure as well as to the backbone and side chain assignment (*33*−*42*). An additional method for selective reverse-protonation is ^{1}H and ^{13}C labeling of the methyl groups of isoleucine, leucine, and valine via addition of specifically labeled biosynthetic precursors to the growth medium (*31*, *43*, *44*). Low-resolution structures of large proteins can be obtained using this approach which was demonstrated by the determination of the global fold of the monomeric 82 kDa protein malate synthase G (*45*).

Despite all recent advances, determination of high-resolution structures by NMR of proteins larger than 35 kDa is very challenging. Of 6124 different protein structures determined by NMR currently deposited in the PDB, only 14 are atomic-resolution structures of systems larger than 35 kDa. Four of these are proteins and protein complexes smaller than 37 kDa (*40*, *42*, *46*, *47*); nine are multimeric proteins (*35*, *48*−*55*), and the remaining one is the 42 kDa maltose binding protein (MBP) that has been extensively studied by crystallography and NMR (*55*). To date, the 65 kDa hemoglobin tetramer is the highest-molecular mass protein complex for which the high-resolution structure has been determined by NMR (*55*). This structure, along with the previously mentioned MBP structure, was recently redetermined by Yang and co-workers using their approach for the determination of the structure of fully protonated large proteins (*55*). This method is based on measuring a combination of 4D ^{13}C, ^{15}N separated NOESY, 3D TROSY-HNCA, and MQ-CCH-TOCSY (*56*) spectra on a uniformly ^{13}C- and ^{15}N-labeled protein without deuteration. The 4D ^{13}C, ^{15}N separated NOESY experiment when used for large unlabeled proteins suffers from a poor signal-to-noise ratio, especially at the low protein concentration used in this study (0.25 mM). Without this 4D spectrum, it is impossible to implement the method described above as it was originally developed. However, several basic concepts from it have been used in this study.

Determination of the structure of protein complexes at atomic resolution relies on obtaining a large number of intermolecular NOEs. Obtaining intermolecular NOEs is a challenging process since it is difficult to distinguish between strong intramolecular and a few weak intermolecular interactions, a problem which is aggravated in large molecules. One way to overcome the obstacle in identifying intermolecular interactions is to label one of the components with ^{15}N and/or ^{13}C while leaving the second component unlabeled. Using isotope filtered-edited experiments, it is possible to identify NOEs across interfaces between two protons, where only one is bonded to a labeled heteroatom (*57*−*61*). However, with the increasing size of protein complexes, these experiments become much less sensitive and require partial or complete deuteration of nonexchangeable protons to achieve a good S/N.

A different approach for the detection of intermolecular NOEs in large protein complexes has been used in several recent studies. It is based on selective ^{1}H and ^{13}C labeling of the I(δ1)LV methyl groups on a deuterated background of one complex component while the other component remains unlabeled or reverse-protonated with several aromatic and/or aliphatic amino acids. The intermolecular NOEs are obtained from a 3D ^{13}C-edited NOESY spectrum by observing the NOEs involving the I(δ1)LV methyl protons (*46*, *62*−*64*).

High-resolution NMR structural studies of the IFNAR2−IFNα2 interactions required further development in methodology, not only because of the size of the complex but also because it is stable only at concentrations no higher than 0.25 mM. In this study, we present a novel approach for the determination of intermolecular side chain−side chain NOEs. Our method is based upon "asymmetric" reverse-protonation of the two complex components on a deuterated background. In one molecule, amino acids with aliphatic side chains are reverse-protonated, and in the other molecule, aromatic amino acids are reverse-protonated. As a result, the aromatic−aliphatic section of the 2D homonuclear NOESY spectrum measured in D_2O shows in principle only cross-peaks originating from intermolecular

interactions. The high sensitivity of the 2D NOESY spectrum, even for large proteins at concentrations as low as 0.25 mM, enables the detection of these interactions with a high S/N. Using this technique, we have been able to obtain 24 intermolecular NOEs which led to a much improved model of the IFNAR2−IFNα2 complex. The model contains a considerable amount of new structural information and reveals a 30° change in the orientation of IFNAR2 relative to IFNα2 in comparison with the previously published model (*26*) as well as a direct involvement of the C domain of IFNAR2 in IFNα2 binding.

EXPERIMENTAL PROCEDURES

Expression of IFNAR2 and IFNα2. Unlabeled and uniformly ^{15}N- and ^{13}C-labeled IFNAR2 and IFNα2 were obtained following previously published expression and purification protocols (*19*, *26*, *65*). Selectively reverse-protonated samples were obtained by adding a 4-fold excess of the selected unlabeled amino acids to otherwise deuterated, ^{15}N-labeled Celtone medium (Spectra Stable Isotopes). The 4-fold excess was calculated with respect to the amount of amino acids present in the deuterated, ^{15}N-labeled Celtone medium. Specifically, unlabeled amino acids His (1.35 mg/mL), Tyr (1.2 mg/mL), Phe (2.4 mg/mL), and Trp (0.61 mg/mL) were used for samples with protonated aromatic residues and Ile (2.9 mg/mL), Val (3.36 mg/mL), Leu (4.57 mg/mL), Met (1.19 mg/mL), Ala (2.9 mg/mL), Lys (4.24 mg/mL), and Thr (2.44 mg/mL) for samples with protonated aliphatic residues. Otherwise, the protocols for expression and purification were used as mentioned above.

NMR Sample Preparation. The IFNAR2−IFNα2 complex as well as free IFNAR2 is stable at pH 8 in 25 mM Tris buffer and 0.02% NaN_3. These measurement conditions are the result of an optimization study which was previously conducted by our group (*19*). IFNα2 is stable at pH 8 only in a ≥500 mM NaCl solution. To make the 1:1 complex (in 10% excess for the unlabeled component), we slowly added 5 mL of concentrated IFNα2 (500 mM NaCl) to 145 mL of dilute IFNAR2 (25 mM NaCl). The volumes and salt concentrations of each component were calculated such that the final salt concentration did not exceed 50 mM. After incubation for 1−2 h at room temperature, the dilute complex was concentrated using Amicon Ultra tubes (Millipore, molecular mass cutoff of 10 kDa). The buffer was exchanged by repeated dilution−concentration cycles to 25 mM d_{11}-Tris (pH 8), 0.02% NaN_3, and 5% D_2O or to 25 mM d_{11}-Tris (pD 8), 0.02% NaN_3, and 98% D_2O. Formation of the complex was verified using an analytical Superdex 75 size exclusion column (Pharmacia). The complex elutes at a volume corresponding to an approximately 44 kDa protein. The final concentration of the complex in all samples was 0.2−0.3 mM. Under these conditions, the NMR samples are stable for 2−3 months at 35 °C, with negligible aggregation or denaturation (*19*).

Deuterium exchange for several IFNAR2−IFNα2 samples was achieved by partial unfolding in 4 M d_4-urea. For this procedure, the complex was dissolved in a D_2O-based unfolding buffer [25 mM Tris (pH 8.0), 4 M d_4-urea, 0.1% protease inhibitor cocktail (Sigma), and 50 mM glycylglycine] to a final concentration of 0.1 mg/mL, incubated for 4 h at room temperature while being shaken gently, and refolded by being dialyzed twice against a 25-fold volume of D_2O-based refolding buffer [25 mM Tris (pH 8.0), 0.1% protease inhibitor cocktail (Sigma), and 50 mM glycylglycine]. To check that the structural integrity of the complex is not compromised by the partial unfolding and refolding procedures, these were performed first on [^{15}N]IFNAR2−IFNα2 and [^{15}N]IFNα2−IFNAR2 samples in H_2O, and the structural integrity was checked by measuring the 2D TROSY ^{1}H−^{15}N HSQC spectra before and after the treatment as well as by size exclusion chromatography.

NMR Measurements. All NMR spectra were recorded at 305 K on a Bruker DRX 800 MHz spectrometer equipped with a 5 mm triple-resonance TCI CryoProbe with *z* gradients and a 5 mm *z* gradient triple-resonance TXI probe. Data were processed and analyzed using NMRDraw/NMRPipe (*66*) and NMRView (*67*).

The 2D TROSY ^{1}H−^{15}N HSQC spectra of free and bound IFNAR2 (numbers in parentheses are for TROSY ^{1}H−^{15}N HSQC spectra of free and bound IFNα2) were recorded using 256 (256) t_1 increments with a sweep width of 1979 (1622) Hz and 1280 (1024) t_2 points with a sweep width of 11161 (10417) Hz. The TROSY ^{1}H−^{15}N HSQC pulse sequence (*68*) was modified to produce greater sensitivity by suppressing the anti-TROSY component without lengthening the pulse sequence or introducing a spin-state selective filter (*69*). The following experiments were conducted for bound IFNAR2 (numbers in parentheses indicate the number of complex points and sweep width in hertz for each dimension): CT ^{1}H−^{13}C HSQC (H, 1280 and 10417; C, 512 and 14085), 3D TROSY HNCA (*55*, *68*, *70*) (H, 1024 and 11161; C, 50 and 4024; N, 106 and 2108), 3D TROSY HNCOCA (*68*, *70*) (H, 1280 and 11161; C, 50 and 4024; N, 100 and 1979), 3D ^{15}N-edited NOESY (H, 1280 and 11161; H, 148 and 8803; N, 78 and 1979), 3D MQ-(H)CCH TOCSY (*71*) (H, 1280 and 11161; C, 68 and 4427; C, 182 and 13280), 3D MQ-(H)CCmHm TOCSY (*72*) (H, 1280 and 8013; C, 122 and 2516; C, 140 and 8299), and 3D (H)CCmHm TOCSY (*71*) (H, 1280 and 7003; C, 122 and 2516; C, 140 and 7003). The following experiments were conducted for free IFNAR2: CT ^{1}H−^{13}C HSQC (H, 2048 and 10417; C, 512 and 14085), 3D ^{15}N-edited NOESY (H, 768 and 11161; H, 160 and 8237; N, 72 and 1946), and 3D MQ-(H)CCmHm TOCSY (*72*) (H, 1280 and 8013; C, 120 and 2516; C, 136 and 8299). The following experiments were conducted for bound and free IFNα2: 3D ^{15}N-edited NOESY (bound IFNα2, H, 1280 and 11161; H, 146 and 8803; N, 78 and 1622) (free IFNα2, H, 1024 and 9615; H, 140 and 8001; N, 72 and 1622). 2D NOESY experiments for all samples were conducted using 400 t_1 increments with a sweep width of 10417 Hz and 1024 t_2 points with a sweep width of 10417 Hz.

An interscan delay of 1.5 s was applied in experiments performed on fully protonated samples, and a delay of 2 s was used for partially deuterated samples. The 3D ^{15}N-edited NOESY experiments were conducted with a mixing time of 100 ms, while the 2D NOESY experiments were conducted with mixing times of 25−200 ms. Water suppression was achieved with the use of flip-back and gradient pulses (*73*, *74*). Residual water magnetization was suppressed using the WATERGATE sequence in the final INEPT transfer to protons immediately before the acquisition of data (*75*). All experiments were optimized for large proteins by applying minimum delays for transverse ^{1}H magnetization and optimal water flip-back pulses. Carrier positions for all experiments were 118.5 ppm for ^{15}N, 174 ppm for ^{13}CO, 54 ppm for ^{13}Cα, 43 ppm for ^{13}Cα/^{13}Cβ, and 4.7 ppm for ^{1}H. Proton decoupling was achieved using WALTZ-16 (*76*) or GARP (*77*) train pulses. Quadrature detection was conducted by acquiring the data in States−TPPI mode (*78*) or Echo−Antiecho (*79*, *80*).

Docking. The docking of the IFNAR2−IFNα2 complex was performed using HADDOCK2.0 (*81*) which utilizes CNS (*82*, *83*). The docking was based on the chemical shift perturbation data for

IFNAR2, the cross-saturation data for IFNα2, NOE interactions, and mutagenesis data (*18*, *19*, *25*, *26*). Starting structures for the docking were the published structures of IFNAR2 [PDB entry 1N6U] (*18*) and IFNα2 [PDB entry 1ITF (*15*)]. Active and passive residues in IFNα2 and IFNAR2 were selected using the strategy outlined by Dominguez et al. (*81*) based on the binding sites mapped in previous studies by our group (*19*, *26*). Solvent accessibility was calculated using NACCESS (*84*, *85*). Additional pairwise distance restraints were defined on the basis of double mutant cycle analysis data conducted by Roisman et al. (*25*). All ambiguous distance restraints were defined with a maximum effective distance of 2 Å. A total of 1000 structures were calculated in the rigid body minimization. Semiflexible simulated annealing followed by refinement in explicit water was performed for the best 200 solutions based on the HADDOCK score (weighted sum of all the energy terms and the buried surface area). Violation analysis of the final 200 structures showed that all the unambiguous distance restraints were maintained for 99.5% of the structures. Solutions were clustered using a 7.5 Å interface rmsd cutoff; 197 of 200 structures were included in the seven clusters found. Cluster analysis was performed on the four best structures in each cluster to remove the dependency of cluster averages upon their size. The cluster with the lowest average HADDOCK score was considered to be the best solution.

Structure Analysis. The structure of the IFNAR2−IFNα2 complex and the interface were analyzed with PISA (protein interfaces, surfaces, and assembly service at the European Bioinformatics Institute) (*86*), CMA (contact map analysis from space, tools for protein structure prediction and analysis based on complementarity and environment) (*87*), and MOLMOL (analysis and display of molecules) (*88*). All molecular pictures were created with Pymol (*89*).

RESULTS

Intermolecular NOEs between IFNAR2 and IFNα2 in the Complex. Aromatic amino acids play an important role in protein−protein interactions. The region of the proton NMR spectrum showing aromatic proton resonances is usually less crowded and better dispersed in comparison to the aliphatic region of the spectrum. Of special interest is the region of the NOESY spectrum showing interactions between aromatic and aliphatic protons. Specific amino acid labeling can be used to assign intermolecular interactions involving aromatic amino acids in large protein complexes as was demonstrated by previous studies in our group (*90*−*94*). In these experiments, we took advantage of the high sensitivity of 2D homonuclear NOESY even for large protein complexes.

The region of a 2D NOESY spectrum of a complex showing aromatic−aliphatic proton interactions can be considerably simplified to show only intermolecular interactions by using asymmetric reverse labeling of the two proteins forming the complex. If one protein is reverse-protonated in the aromatic amino acids on a perdeuterated background and the other protein is reverse-protonated in selected aliphatic amino acids on a perdeuterated background, the upper left quarter of the complex 2D NOESY spectrum in D_2O will show, in principle, intermolecular interactions between aromatic and aliphatic amino acids as well as intraresidue interactions between the aromatic protons and the α- and β-protons of these amino acids. If preliminary data about the interface of the complex are available, the aliphatic amino acids can be reverse-labeled according to the expected interactions to reduce costs and the number of samples to be prepared.

The aromatic amino acids at the mapped binding site of IFNAR2 include residues ^{R2}H76, ^{R2}Y79, ^{R2}H97, ^{R2}F99, and ^{R2}W100, while those at the binding site of IFNα2 include residues $^{\alpha2}$F27, $^{\alpha2}$F36, $^{\alpha2}$F38, $^{\alpha2}$W140, and $^{\alpha2}$F151. Aromatic amino acids are usually involved in hydrophobic interactions and sometimes also in cation−π interactions with arginine and lysine residues. On the basis of the previous mapping of the IFNα2 and IFNAR2 binding sites (*19*, *26*), we prepared two samples of the IFNα2−IFNAR2 complex. One sample was reverse-protonated with the unlabeled aromatic amino acids histidine, phenylalanine, and tryptophan for IFNAR2 and reverse-protonated with the unlabeled aliphatic amino acids lysine, arginine, leucine, alanine, and methionine for IFNα2 [this sample will hereafter be termed IFNAR2(HFW)−IFNα2(KRLAM)]. The second sample was reverse-protonated with the unlabeled aliphatic amino acids isoleucine, valine, leucine, threonine, methionine, alanine, and lysine for IFNAR2 and reverse-protonated with the unlabeled aromatic amino acids histidine, phenylalanine, and tryptophan for IFNα2 [IFNAR2(IVLTMAK)−IFNα2(HFWY)]. The reverse-protonation of all proteins was conducted on a ^{15}N-labeled, deuterated background.

The labeling scheme was verified using ^{15}N HSQC and 2D NOESY spectra determined for the free proteins in H_2O and in D_2O, respectively, prior to formation of the complex. No significant signs of scrambling were observed in these spectra which we attribute to the expression of the proteins in rich media in which all amino acids are essentially already present; therefore, their de novo production is minimized.

2D NOESY spectra of the asymmetrically labeled samples in D_2O were measured, and a large number of cross-peaks were observed in the aromatic−aliphatic region, many more than were expected on the basis of the previous model of the complex (*26*) (Figure 1 and Figure 1S of the Supporting Information). The initial assumption was that many of the observed spin systems originate from amide protons that did not exchange with the solvent because they were buried. These amide protons could interact with the reverse-labeled aliphatic protons of the same protein and contribute to the observed signal in the asymmetrically labeled complex. To rid the aromatic region of the 2D NOESY spectrum of NOEs originating from amide protons, a rigorous D_2O exchange protocol was used. Both asymmetrically labeled samples [IFNAR2(HFW)−IFNα2(KRLAM) and IFNAR2(IVLTMAK)−IFNα2(HFWY)] were partially unfolded in 4 M d_4-urea in a D_2O solution and then refolded by dialysis against the D_2O NMR buffer. The structural integrity of the samples after refolding was confirmed by size exclusion chromatography and 2D TROSY ^{1}H−^{15}N HSQC spectra (see Experimental Procedures) as well as by comparison of the 2D NOESY spectra before and after the urea treatment (Figure 1S of the Supporting Information). 2D NOESY spectra of IFNAR2(HFW)−IFNα2(KRLAM) and IFNAR2(IVLTMAK)−IFNα2(HFWY) measured before and after the urea treatment revealed that numerous NOE cross-peaks with amide protons disappeared (see Figure 1S of the Supporting Information).

However, despite the complete elimination of amide proton cross-peaks, several unexplained spin systems with narrow line widths still remained in the 2D NOESY spectra along with spin systems that could originate from aromatic protons (Figure 1). Consequently, 2D NOESY spectra of each of the reverse-labeled complex components in their free form were measured to examine whether these narrow cross-peaks could arise from

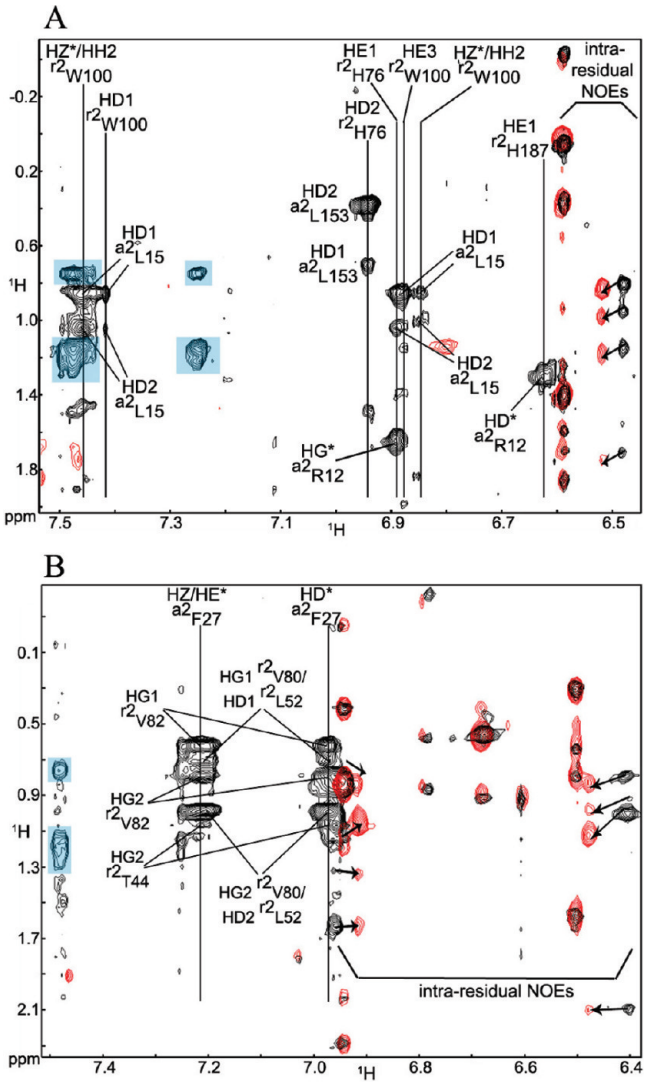

FIGURE 1: Intermolecular NOE interactions in the IFNAR2−IFNα2 complex detected in the asymmetrically labeled complex. (A) Overlay of 2D NOESY spectra in D_2O of IFNAR2-(HFW)−IFNα2(KRLAM) (black) and IFNα2(KRLAM) (red). (B) Overlay of 2D NOESY spectra in D_2O of IFNAR2(IVLTMAK)−IFNα2(HFWY) (black) and IFNAR2(IVLTMAK) (red). Red cross-peaks originate from intramolecular interactions. Arrows indicate minute changes in the positions of the intramolecular cross-peaks between the spectra of the free molecule and the complex. Black cross-peaks not overlaid with red cross-peaks and not marked by arrows originate from intermolecular interactions and are labeled according to the assignment of the aliphatic proton. Vertical lines indicate spin systems of cross-peaks originating from the same aromatic proton and are labeled according to the assignment of the specific proton. Light blue boxes indicate cross peaks that appeared after the urea-induced partial denaturation.

intramolecular interactions. Surprisingly, several cross-peaks in the aromatic−aliphatic region were observed (Figure 1). As one can see from the overlay of 2D NOESY spectra of the IFNAR2-(HFW)−IFNα2(KRLAM) complex and free IFNα2(KRLAM) (Figure 1A), two spin systems that appear in the aromatic−aliphatic region of both spectra obviously result from intramolecular NOEs of IFNα2 and not intermolecular NOEs between IFNα2 and IFNAR2. These spin systems have a distinct narrow line width in comparison to those of other, much broader peaks in the same spectral region. This might indicate that these NOE peaks result from isolated ^{1}H spins not surrounded by protons of the same residue. We postulate that while the majority of protein molecules in the IFNα2(KRLAM) sample were labeled with ^{1}H only as designed (i.e., only in aliphatic amino acids), a small percentage of ^{1}H labels were randomly incorporated in all amino acid types. This might be due to the incomplete ^{2}H labeling of the commercially available expression medium (97% instead of 100%). In a highly deuterated environment, even a small amount of protons will give an observable signal, simply because their transverse relaxation times are much longer and the magnitude of the ensuing signal is considerably larger because of its narrow line width. A second possibility is scrambling resulting from the unlabeled aliphatic amino acids that were added to the growth medium.

Following the replacement of the slowly exchanging amide protons with deuterium using urea-induced partial denaturation, several new spin systems appeared in the 2D NOESY spectra of the urea-treated samples (marked by light blue boxes in Figure 1). A possible explanation for these cross-peaks is a minor chemical modification as a consequence of the urea-induced unfolding, for example, a carbamylation of lysine residues by the cyanate ion resulting from urea decomposition. Since the ^{15}N HSQC spectra of the IFNα2−IFNAR2 complex refolded in H_2O (see Experimental Procedures) remained the same before and after the urea treatment as have the other cross-peaks in the 2D NOESY spectra, this modification did not interfere to any significant extent with the structure of the complex and the binding of the two proteins.

The few spin systems that remain in the aromatic−aliphatic region of the 2D NOESY spectra of the asymmetrically labeled samples after elimination of the intramolecular NOEs and the cross-peaks resulting from the urea-induced modification are the intermolecular NOEs between aromatic protons of IFNα2 and aliphatic protons of IFNAR2 and vice versa. Using these NOE cross-peaks as distance restraints requires the identification of the specific protons involved in the interaction, i.e., obtaining side chain proton assignments of the IFNAR2−IFNα2 complex. The side chain and backbone assignment of the IFNAR2−IFNα2 complex will be discussed in the following sections.

Backbone Assignment of IFNAR2 in Complex with IFNα2. The side chain proton assignment process is not trivial for a complex of 44 kDa and is further complicated by the low concentration and high pH at which the complex is stable. While backbone assignment for proteins this size is usually obtained with perdeuterated samples, we used nondeuterated samples by applying several basic principles from the assignment method recently developed by Yang and co-workers for fully protonated large proteins (*55*).

The assignment process began with the use of the 3D TROSY-HNCA and 3D TROSY-HN(CO)CA spectra to find candidates to be HN($i-1$) by matching the inter-residual Cα chemical shift of HN(i) to intraresidue Cα chemical shifts of other amide pairs. Since the ^{13}C chemical shifts of the Cα atoms suffer from low dispersion, there are likely to be several such candidates. This problem is resolved by using the 3D ^{15}N-edited NOESY spectrum. Interproton distance statistics indicate that amides i and j are more likely to have a sequential relationship when amide i shares a larger number of common NOEs with amide j than with other amides. The probability that two nonadjacent amides share the largest number of common NOEs, and have matching Cα chemical shifts in their HNCA correlations, is very low (*55*). Following this observation, an NOE score is calculated for each of the candidates by comparing their 3D ^{15}N-edited NOESY strips with that of HN(i) and summing up the number of NOE cross-peaks that have the same ^{1}H chemical shifts within a specified

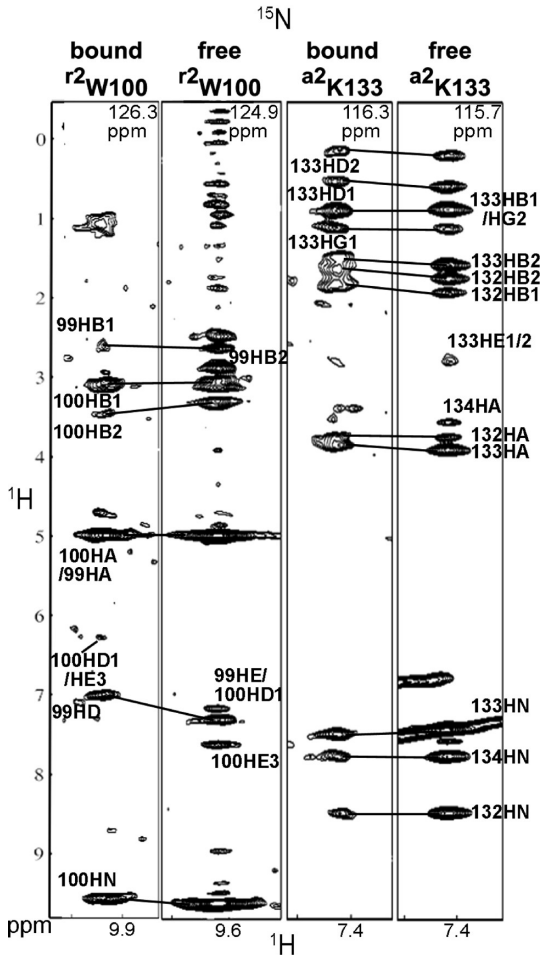

FIGURE 2: $^{1}H-^{15}N$ strips from 3D ^{15}N-edited NOESY spectra of free and bound IFNAR2 and free and bound IFNα2. NOESY strips of ^{R2}W100 and $^{\alpha 2}$K133 for which the side chain assignment was based on the side chain assignment of free IFNAR2 and free IFNα2. Bound r2 and free r2 stand for bound and free IFNAR2, respectively, while bound a2 and free a2 stand for bound and free IFNα2, respectively. The strips are marked with the chemical shift of the amide nitrogen.

tolerance. The candidate with the highest NOE score is considered to be HN($i-1$).

By using the strategy outlined above, we confirmed the previously achieved 85% of backbone amide assignment for IFNAR2 in complex with IFNα2 (*19*) and added the assignment of 87% of the Cα resonances (of the fully protonated bound IFNAR2).

Side Chain Assignment of IFNAR2 in the IFNAR2−IFNα2 Complex Using ^{15}N-Edited NOESY. Side chain proton assignment relied on the ^{15}N-edited NOESY spectrum of the complex and its similarity to the same spectrum measured for free IFNAR2 (Figure 2).

For residues not found in the binding site for IFNα2, it is quite simple to transfer ^{1}H assignments from free to bound IFNAR2. As for residues that are part of the binding surface, a transfer of assignment is also possible for a number of reasons. First, Hα and Hβ protons do not change their chemical shift significantly since the interactions in the binding site usually involve side chain protons other than the α- and β-protons. Second, since these residues are mainly situated in loops (*19*), the number of intramolecular nonsequential inter-residual cross-peaks in their ^{15}N NOESY strips is very small. Third, not many intermolecular NOEs originating from amides of IFNAR2 are expected to appear in the spectrum since those are usually located farther from the binding interface which is created primarily by side chains. Therefore, most NOESY strips of interface amides consist of intraresidual NOEs and sequential inter-residual NOEs that did not significantly change their chemical shift upon binding, making the assignment transfer fairly easy as one can see in Figure 2 for IFNAR2 residue W100 which is located in the binding interface. In summary, more than 50% of the side chain protons were assigned for 87% of the residues in bound IFNAR2 using the method outlined above. Only 10% of residues in bound IFNAR2 do not have any side chain ^{1}H assignment.

Side Chain Assignment for Methyl-Containing Residues of IFNAR2 in the IFNAR2−IFNα2 Complex. MQ-(H)CC$_m$H$_m$ TOCSY, MQ-(H)CCH TOCSY, and H(C)C$_m$H$_m$ TOCSY (*71*) experiments were used to assign side chain ^{13}C and ^{1}H resonances in methyl-containing residues of IFNAR2 in complex with IFNα2. MQ-(H)CC$_m$H$_m$ TOCSY and H(C)C$_m$H$_m$ TOCSY experiments correlate chemical shifts of methyl carbons and protons with chemical shifts of all side chain carbons or protons in the same residue. Hence, side chain assignment of methyl-containing residues is possible if assignments for the methyl protons and carbons are available, i.e., the CT ^{13}C HSQC spectrum of the methyl region is assigned. Comparison of the CT ^{13}C HSQC spectrum of free [^{13}C,^{15}N]IFNAR2 with that of [^{13}C,^{15}N]-IFNAR2 bound to unlabeled IFNα2 showed that ~85% of the methyl group cross-peaks did not change their chemical shift upon IFNα2 binding to any significant extent (Figure 3A). Cross-peaks showing considerable chemical shift changes originated from methyl groups of residues previously identified as situated in the binding site (*19*). Consequently, many resonance assignments could be transferred from the methyl groups of free IFNAR2 to the methyl groups of bound IFNAR2. For methyl groups located at the binding interface, it was in most cases possible to identify the shifted peaks in the CT ^{13}C HSQC spectrum of bound IFNAR2 (Figure 3A). All assignments were validated by verifying that the corresponding MQ-(H)CC$_m$H$_m$ TOCSY strip showed the appropriate spin system type pattern and the Cα chemical shift matched the one found from the HNCA spectrum (see Backbone Assignment of IFNAR2 in Complex with IFNα2). Furthermore, for Ile, Leu, and Val residues, a match was confirmed between the strips originating from each of the two methyl groups.

Once methyl protons were identified, the other carbon or proton resonances of the spin system could be assigned using the MQ-(H)CC$_m$H$_m$ TOCSY and H(C)C$_m$H$_m$ TOCSY spectra (Figure 3B). The assignment was facilitated by the MQ-(H)CCH TOCSY spectrum in cases of weak signals in the MQ-(H)CC$_m$H$_m$ TOCSY spectrum. The non-CT MQ-(H)CCH TOCSY experiment has a lower resolution than the CT MQ-(H)CC$_m$H$_m$ TOCSY experiment; however, the former is significantly more sensitive (*71*). This difference in sensitivity is especially pronounced for leucine residues with strong scalar coupling interactions which give rise to a low S/N in the MQ-(H)CC$_m$H$_m$ TOCSY spectrum because their ^{13}C magnetization cannot be refocused completely during the CT period (*71*). Assignment of side chain carbons was achieved for more than 90% of the methyl-containing residues.

Side chain protons were assigned using the H(C)C$_m$H$_m$ TOCSY spectrum and were in agreement with the assignments based on ^{15}N-edited NOESY spectra for all methyl-containing residues for which they were available. In most cases, we were able to complete the side chain proton assignment of methyl-containing residues.

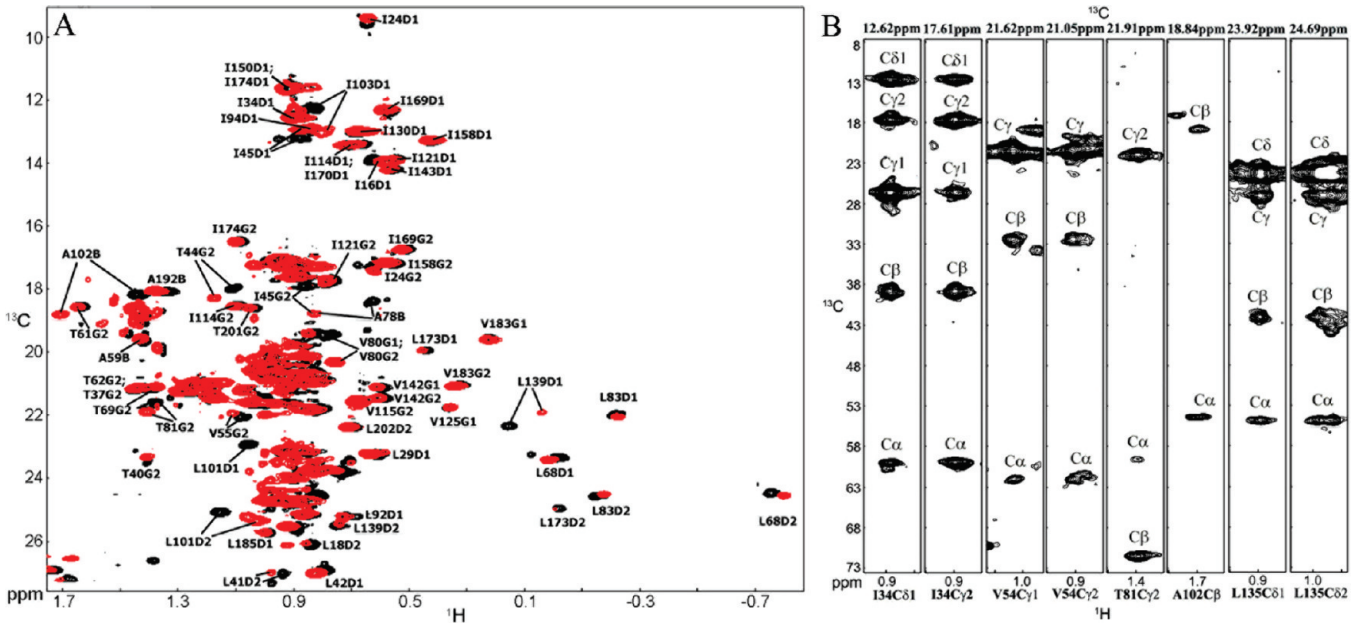

FIGURE 3: Side chain assignment of methyl-containing residues of bound IFNAR2. (A) Overlay of CT ^{13}C HSQC spectra of free IFNAR2 (black) and IFNAR2 bound to unlabeled IFNα2 (red). (B) MQ-(H)CC$_m$H$_m$ TOCSY strips of IFNAR2 in complex with IFNα2. Representative strips of five methyl-containing residues (Ile, Val, Thr, Ala, and Leu) are shown. The strips are marked with the chemical shift of the methyl carbon.

Side Chain Assignment of IFNα2 in the IFNAR2−IFNα2 Complex. Backbone assignment of bound IFNα2 was accomplished previously in our group using uniform ^{13}C, ^{15}N, and ^{2}H labeling and TROSY multidimensional NMR spectra (*26*).

Side chain proton assignment of bound IFNα2 was achieved via comparison of ^{15}N-edited NOESY strips of free IFNα2 to those of bound IFNα2 in a manner similar to that described for bound IFNAR2 (Figure 2). This comparison resulted in > 50% proton side chain assignment for 80% of bound IFNα2 residues despite the fact that the spectra of the free and bound forms were not measured under the same pH conditions. The NMR spectra were measured under different conditions since free IFNα2 is stable at an acidic pH of 3.5 and the IFNAR2−IFNα2 complex is stable at a slightly basic pH of 8.0. Therefore, the amide resonances, which are strongly influenced by pH, radically change their positions, and the ^{15}N HSQC spectra of free and bound IFNα2 are very different. However, aliphatic protons are not greatly influenced by changes in the solution pH, making it possible to compare their positions under different pH conditions. Since the amide backbone assignment for both free and bound IFNα2 is available from previous studies (*15*, *26*), strips of the ^{15}N-edited NOESY spectrum of each form of IFNα2 were prepared according to their individual HN sequential assignment, and the chemical shifts of the aliphatic protons in each HN strip were compared between free and bound IFNα2.

Assignment of Intermolecular NOEs between IFNAR2 and IFNα2. Assignment of the cross-peaks in the 2D NOESY spectra of the asymmetrically labeled samples (Figure 1) was enabled by the proton side chain assignment of the IFNα2−IFNAR2 complex described above and greatly facilitated by the docking model of the complex previously calculated by Quadt-Akabayov et al. (*26*).

For the 2D NOESY spectrum of IFNAR2(IVLTMAK)−IFNα2(HFWY) (Figure 1B), the assignment was quite straightforward since there are cross-peaks of only two aromatic protons in this spectrum and both interact with the same aliphatic protons. These two aromatic protons give NOEs to each other, indicating that they belong to the same aromatic residue. The aromatic residue was identified as $^{\alpha2}$F27 in IFNα2 on the basis of the cross-peaks with Hβ and Hα protons for which sequential assignment has been obtained. The aliphatic protons were assigned to the methyl protons of ^{R2}V80, ^{R2}V82, ^{R2}L52, and ^{R2}T44 in IFNAR2 according to their chemical shifts.

Assignment of the intermolecular NOEs in the 2D NOESY spectrum of IFNAR2(HFW)−IFNα2(KRLAM) (Figure 1A) was more complicated because of incomplete side chain assignment for aromatic residues of IFNAR2 and aliphatic residues of IFNα2. Another asymmetrically labeled sample was prepared to assist the assignment process. This sample contained deuterated IFNα2 reverse-labeled with protonated leucine residues bound to deuterated IFNAR2 reverse-labeled with protonated tryptophan and histidine residues [IFNAR2(WH)−IFNα2(L)]. Figure 4 shows an overlay of the 2D NOESY spectra of IFNAR2-(HFW)−IFNα2(KRLAM) (black) and IFNAR2(WH)−IFNα2-(L) (red). All but two cross-peaks in the aromatic−aliphatic region of the IFNAR2(HFW)−IFNα2(KRLAM) spectrum could be superimposed with cross-peaks in the IFNAR2(WH)−IFNα2-(L) spectrum (Figure 4). The cross-peaks appearing in both spectra represent NOEs that originate from ^{R2}W−$^{\alpha2}$L and/or ^{R2}H−$^{\alpha2}$L interactions, and cross-peaks appearing only in the IFNAR2(HFW)−IFNα2(KRLAM) spectrum represent NOEs involving either phenylalanine, lysine, arginine, alanine, or methionine residues.

According to the previous IFNα2−IFNAR2 docking model, the best candidates for the interactions between IFNAR2 tryptophan and/or histidine residue and IFN-α2 leucine residues (^{R2}W^{R2}-H−$^{\alpha2}$L) are ^{R2}W100 and ^{R2}H76 in IFNAR2 and $^{\alpha2}$L15 and $^{\alpha2}$L153 in IFNα2. Four spin systems of the six common to both the IFNAR2(HFW)−IFNα2(KRLAM) and IFNAR2(WH)−IFNα2(L) spectra were assigned to the aromatic protons of ^{R2}W100 by matching the Hα, Hβ, and Hδ chemical shifts to the previously obtained proton side chain assignments of bound IFNAR2. All of these interact with a single leucine residue which

can be seen in the spectrum (Figure 1A). However, it was impossible to identify which Leu residue it is, since neither $^{\alpha2}$L15 nor $^{\alpha2}$L153 was assigned. Two of the remaining ^{R2}W−$^{\alpha2}$L and/or ^{R2}H−$^{\alpha2}$L interactions were assigned to ^{R2}H76 by the elimination since ^{R2}H76 also lacks assignment. To decide which aromatic residue (^{R2}H76 or ^{R2}W100) interacts with which Leu residue ($^{\alpha2}$L15 or $^{\alpha2}$L153), two docking models of the IFNα2−IFNAR2 complex (see the next section) were calculated using HADDOCK (*81*): one with distance restraints between ^{R2}W100 and $^{\alpha2}$L15 and between ^{R2}H76 and $^{\alpha2}$L153 and the other with distance restraints between ^{R2}W100 and $^{\alpha2}$L153 and between ^{R2}H76 and $^{\alpha2}$L15. A comparison between the two models revealed that the ^{R2}W100−$^{\alpha2}$L15 and ^{R2}H76−$^{\alpha2}$L153 configuration of interactions is much more energetically favorable (intermolecular energy of −379.29 kcal/mol compared to −136.49 kcal/mol for the second option). Furthermore, when these docking models were analyzed, it was quite clear that ^{R2}H76 interacts both with $^{\alpha2}$L153 and with $^{\alpha2}$L15 using one of its two aromatic protons for each respective interaction (i.e., Hδ interacts with $^{\alpha2}$L153 and Hε interacts with $^{\alpha2}$L15) (Figures 4 and 5B). This observation was also found to be supported by the spectrum (Figure 1A).

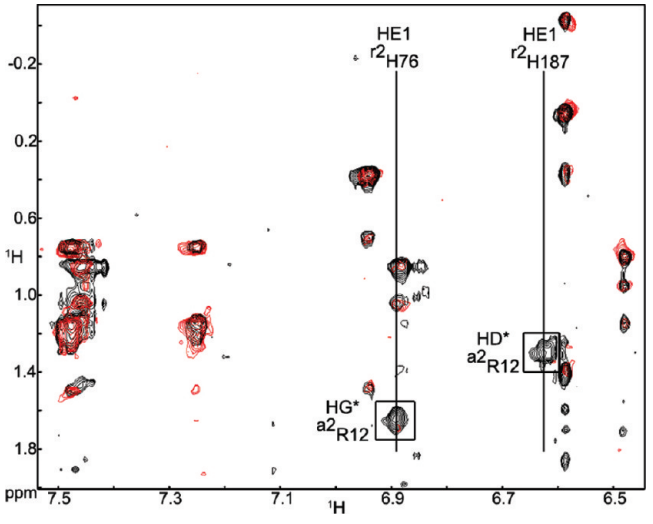

FIGURE 4: Assignment of intermolecular interactions involving IFNAR2 histidine residues. Overlay of 2D NOESY spectra in D_2O of IFNAR2(HFW)−IFNα2(KRLAM) and IFNAR2(WH)−IFNα2(L) (red). Black boxes indicate cross-peaks that do not originate from an NOE between aromatic protons of Trp or His and aliphatic protons of Leu and are labeled according to the assignment of the aliphatic proton. Vertical lines indicate spin systems of cross-peaks originating from the same aromatic proton and are labeled according to the assignment of the specific proton.

On the basis of the new docking model which included all the interactions assigned so far, we were able to identify the two remaining intermolecular NOE cross-peaks in the IFNAR2-(HFW)−IFNα2(KRLAM) spectrum which were not derived from an ^{R2}W−$^{\alpha2}$L or ^{R2}H−$^{\alpha2}$L interaction (Figure 4). One of these is assigned to the interaction between Hε of ^{R2}H76 and Hγ of $^{\alpha2}$R12 on the basis of the model and ambiguous proton chemical shift assignment from the ^{15}N-edited NOESY spectrum. According to the docking model, the only possible interaction which could give rise to the last unassigned cross-peak in the IFNAR2(HFW)−IFNα2(KRLAM) spectrum is between Hε of ^{R2}H187 and Hδ of $^{\alpha2}$R12 and hence was assigned as such (Figure 4).

Stereospecific assignment of the cross-peaks originating from the methyl groups of Leu and Val residues was obtained from the docking model containing the ambiguous restraints via assignment of the stronger NOE cross-peaks to the proton pairs situated closer to each other.

Docking Model of the IFNAR2−IFNα2 Complex. A docking model of the IFNα2−IFNAR2 complex was calculated previously by our group on the basis of the NMR mapping of the binding sites on both proteins, double mutant cycle restraints, and a single intermolecular NOE (*26*). Here, our goal was to use the 24 intermolecular NOEs found in this study to improve the existing model on the basis of a much larger number of intermolecular NOE interactions. A reliable model of a complex can be calculated on the basis of the structures of its free components, provided that these do not undergo major structural changes as a result of binding. Both IFNAR2 and IFNα2 satisfy this condition since their global and secondary structures are maintained upon binding and any conformational changes that do occur are restricted to the binding site region (*19*, *26*).

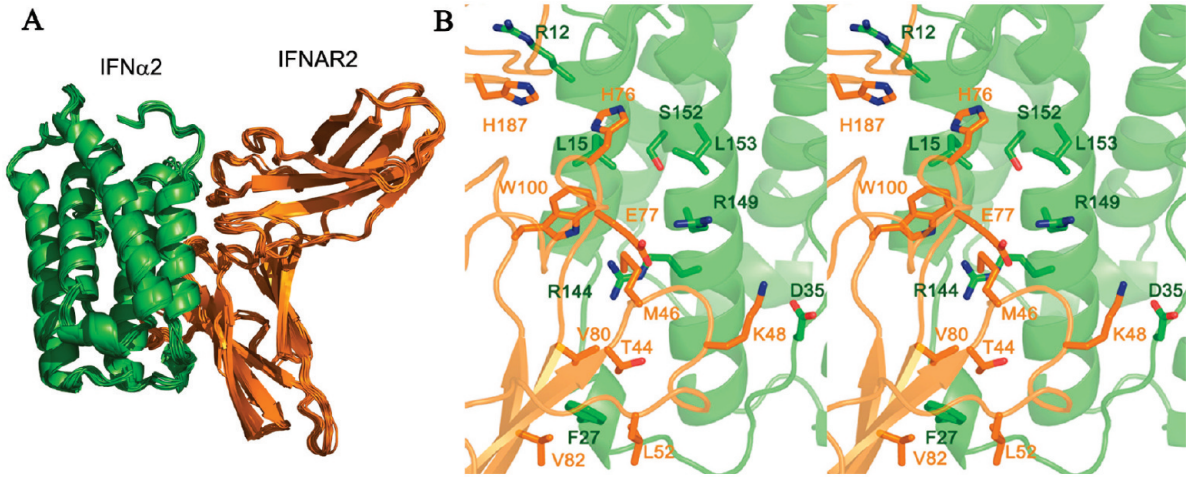

FIGURE 5: Docking model of the IFNAR2−IFNα2 complex based on intermolecular NOEs. (A) Ensemble of the 10 best structures from the highest-ranking cluster in the calculation. IFNAR2 is colored orange and IFNα2 green. The flexible N-terminal (^{R2}S1−^{R2}C12) and C-terminal (^{R2}P204−^{R2}S212) residues of IFNAR2 were removed for the presentation. (B) Stereo representation of an interface close-up of the docking model of the IFNAR2−IFNα2 complex. Residues involved in the intermolecular NOEs or DMC interactions and used in the docking are depicted as sticks. IFNAR-EC is colored orange and IFNα2 green.

Table 1: Intermolecular Restraints Used in the Docking Procedure[a]

AIR	IFNAR2	
	active	M46, S47, K48, P49, E50, D51, L52, K53, V54, S74, H76, E77, V80, V82, C95, S96, H97, N98, W100, I103, D104
	passive	S11, T13, K15, L42, T44, V55, R73, L83, E84, G85, S94, M105, L135, Q136, D138, L139, L141, L185, H187, S188, D189, Q191
	flexible segments	9−17, 40−57, 71−87, 92−107, 133−143, 183−193
	IFNα2	
	active	L26, F27, S28, C29, L30, K31, R33, H34, D35, F36, G37, F38, W140, A145, M148, R149, S152, L153
	passive	R12, M16, A19, R22, I24, S25, Q40, E41, A118, K121, R125, L128, E132, K133, S136, P137, C138, N156, E159, S160
	flexible segments	10−43, 116−162
DMC	IFNα2	IFNAR2
	D35 OD*	K48 NZ
	R144 HG* or HD*	M46 HG* or HE*
	R149 HN*	E77 OE*
	S152 OG	H76 NE1 or NE2
NOE	IFNα2	IFNAR2
	D35 HN	K48, all nonlabile side chain protons
	F27 HZ, HE, or HD**	*V80 HG**
	F27 HZ, HE, or HD**	*L52 HD**
	F27 HZ, HE, or HD**	*V82 HG**
	F27 HZ, HE, or HD**	*T44 HG2**
	*L15 HD**	*W100, all aromatic protons*
	*L153 HD**	*H76 HD2*
	*L15 HD**	*H76 HE1*
	*R12 HG**	*H76 HE1*
	*R12 HD**	*H187 HE1*

[a]Intermolecular NOEs used in the previous model are in regular font, and the NOEs added in the current model are in italics.

In silico docking of IFNAR2 and IFNα2 was performed using HADDOCK which allows the input of experimental restraints to drive the docking calculation (*81*). The 21 active and 22 passive residues in IFNAR2 (Table 1) as well as the 18 active and 20 passive residues in IFNα2 (Table 1) were selected on the basis of the strategy outlined by Dominguez et al. (*81*) from the previous NMR mapping of the binding sites (*19*, *26*). The experimental intermolecular distance restraints employed in the calculation include all the restraints used in the previous model (*26*), with the addition of all the intermolecular NOEs found in this study (Table 1). A total of 1000 structures were calculated in the rigid body minimization. Semiflexible simulated annealing followed by refinement in explicit water was performed for the 200 best solutions based on the HADDOCK score (weighted sum of all the energy terms and the buried surface area). Violation analysis of the final 200 structures showed that all the NOE−DMC distance restraints were maintained for 99.5% of the structures. Solutions were clustered using a 7.5 Å interface rmsd cutoff; 197 of 200 structures were included in the seven clusters found. Cluster analysis was performed on the four best structures in each cluster to remove the dependency of cluster averages upon their size. The cluster with the lowest average HADDOCK score was considered to be the best solution. The rmsd of the ensemble of the 10 best structures of the best cluster is 0.8 ± 0.1 Å for the backbone atoms and 1.1 ± 0.1 Å for all heavy atoms (Figure 5A). The average intermolecular energy of this ensemble is −391 ± 45 kcal/mol, and the average buried surface area is 3060 ± 129 Å^2 (Table 2). A close-up view of the binding interface shows the side chain orientation of all residues involved in the NOE−DMC distance restraints used in the docking calculation of the current model (Figure 5B).

As shown in Figures 6 and 7 and in Table 3, the area of the binding sites on IFNα2 and IFNAR2 has increased by ~2-fold, compared to the previous two models [Chill et al. (*18*) and Quadt-Akabayov et al. (*26*)]. Most importantly, this study reveals that the binding site on each protein is composed of two major parts, each contributing roughly half of the binding surface area. The upper section of the binding site in the two proteins which was revealed in previous studies (*18*, *26*) consists of a striated motif of matching hydrophobic patches flanked by two stripes of polar residues arranged in an alternating charge pattern creating complementary electrostatic interactions. The lower section of the binding site, revealed in this study, consists almost exclusively of an electrostatically complementary mosaic pattern of charged and polar residues. The upper section of the binding site incorporates residues from helices A and E and the A−B loop of IFNα2 and from the S3−S4 and S5−S6 loops, the interdomain loop (S7−S8), and small parts of the S3 and S6 strands of IFNAR2 (Figures 6 and 7). The lower section of the interface consists of the N-terminus and beginning of helix A as well as the C-terminus of IFNα2 and residues from several loops (S9−S10, S11−S12, and S13−S14) from the C domain of IFNAR2 (Figures 6 and 7).

Most of the charged or polar residues situated in the binding interface participate in hydrogen bonds or salt bridges with residues from the other protein. Eleven intermolecular salt bridges and 12 hydrogen bonds are formed between IFNAR2 and IFNα2 in at least five of the 10 structures in the ensemble (Table 4).

DISCUSSION

Determination of Intermolecular NOEs between IFNAR2 and IFNα2 in the Complex. The main focus in structural studies of protein complexes is the intermolecular interactions that are formed when the two molecules bind each other. Heteronuclear experiments used to detect intermolecular interactions suffer from a poor signal-to-noise ratio when applied

Table 2: Docking and Structural Statistics for the 10 Best IFNAR2−IFNα2 Model Structures[a]

	ensemble	representative structure
docking statistics		
HADDOCK score	−135 ± 9	−133
E_{vdw} (kcal/mol)	−94 ± 10	−94
E_{elec} (kcal/mol)	−552 ± 46	−529
E_{inter} (kcal/mol)	−391 ± 45	−375
E_{AIR} (kcal/mol)	254 ± 16	248
BSA (Å^2)	3060 ± 129	2949
rmsd from lowest-energy structure (Å)	0.69 ± 0.25	0.64
cluster size	60	−
no. of AIR violations >0.3 Å	8 ± 1	8
no. of NOE or DMC violations >0.3 Å	0	0
structural statistics		
rmsd for backbone (heavy atoms) (Å)	0.76 ± 0.1 (1.08 ± 0.08)	−
rmsd for all atoms at interface (Å)	1.49 ± 0.1	−
rmsd for backbone (heavy atoms) from free IFNAR-EC (Å)	0.99 ± 0.04 (1.42 ± 0.04)	0.95 (1.41)
rmsd for backbone (heavy atoms) from free IFNα2 (Å)	0.73 ± 0.08 (1.15 ± 0.06)	0.66 (1.09)
deviations from idealized geometry		
rmsd for bond angles (deg)	0.6	0.6
rmsd for bond lengths (Å)	0.004	0.004
Ramachandran analysis		
residues in most favored regions (%)	79.1	78.1
residues in additionally allowed regions (%)	19.4	20.3
residues in generously allowed regions (%)	0.6	0.9
residues in disallowed regions (%)	0.9	0.7

[a]Structure validation parameters were calculated using PSVS [Protein Structure Validation Software suite (*102*)].

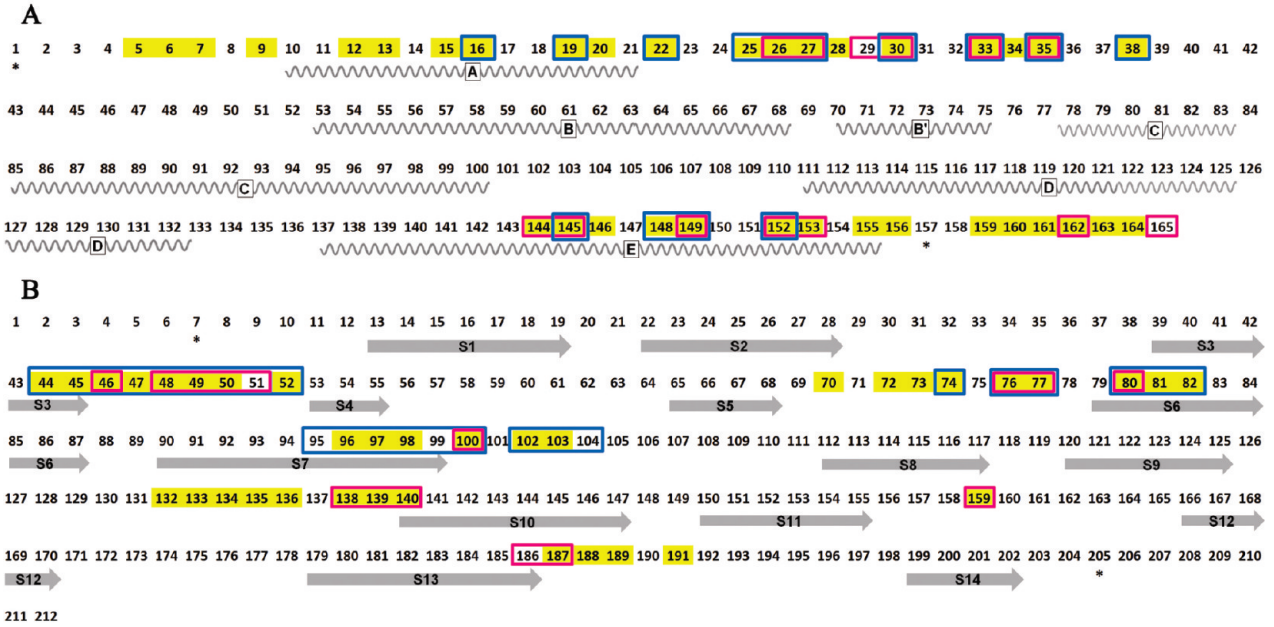

FIGURE 6: Summary of binding site residues in the current and previous docking models of the IFNAR2−IFNα2 complex. (A) IFNα2 residues and (B) IFNAR2 residues situated in the binding site of the current model are highlighted in yellow. Interface residues correspond to a minimal set determined by PISA (*86*), CMA (*87*), and MOLMOL (*88*) with an intermolecular distance criterion of ≤4 Å and are shown if present in at least five of the 10 structures in the ensemble. Residues in the interface of the Quadt-Akabayov et al. model (*26*) are marked with magenta boxes, while residues in the interface of the Chill et al. model (*18*) are marked with blue boxes. Asterisks mark the beginning and end of the IFNα2 and IFNAR2 sequences present in the Chill et al. model (*18*). Secondary structure elements (helices or sheets) are shown in graphic representation marked with their names.

to large protein complexes. However, homonuclear 2D NOESY spectra retain considerable sensitivity even for large protein complexes. Difference spectra along with specific deuteration of proteins can be used to simplify the crowded and unresolved 2D spectra and obtain information about intermolecular interactions even for large protein complexes (>50 kDa). These difference spectra, with the aim of obtaining structural information about the binding interface, are usually very well resolved (*90*, *94*−*96*) despite the size of the proteins; however, they suffer from subtraction artifacts as a result of measurements taken with two different samples.

In this study, a novel approach for the observation of intermolecular side chain−side chain NOE interactions in large protein complexes has been applied. This method is based on

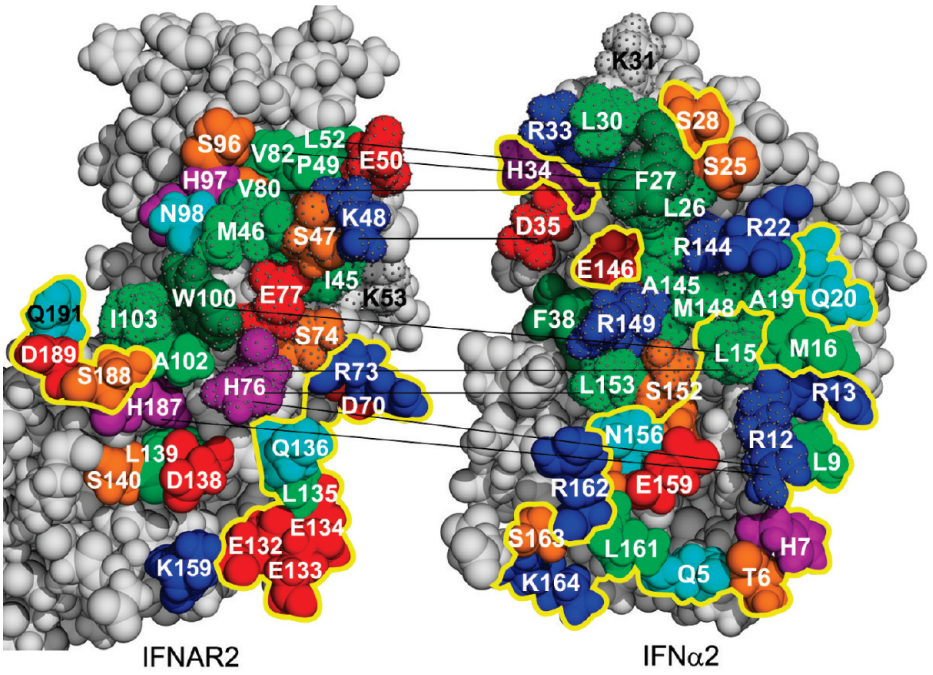

FIGURE 7: Open book representation of the IFNAR2−IFNα2 complex and the observed NOE interactions. IFNAR2 (left) and IFNα2 (right) are presented in space-filling mode. Colored residues were found to be part of the binding interface in the current model according to the analysis depicted in Figure 6. Residues are colored light green for aliphatic, dark green for aromatic, red for negatively charged, blue for positively charged, cyan for Asn and Gln, indigo for His, and orange for Ser and Thr. Residues marked with dots were determined by mutagenesis studies to be important for binding. Residues giving rise to the observed intermolecular NOEs used in the docking calculation are connected with black lines. Yellow contour lines include residues added to the binding interface in this study.

Table 3: Comparison between the Structural Statistics of the Different Models of the IFNAR2−IFNα2 Complex

	Quadt-Akabayov et al. model (*26*)	Chill et al. model (*18*)	current model[a]
no. of IFNAR2 residues in the interface	15	24	36
no. of IFNα2 residues in the interface	13	14	35
buried surface area on IFNAR2 (Å^2)	740	800	1556
buried surface area on IFNα2 (Å^2)	801	650	1611
no. of intermolecular hydrogen bonds	4	2	12
no. of intermolecular salt bridges	8	6	11

[a]The number of residues in the interface was determined as described in the legend of Figure 7. The number of salt bridges and hydrogen bonds was determined as described in Table 4. The buried surface area was calculated using PISA [protein interfaces, surfaces, and assembly service of the European Bioinformatics Institute, authored by E. Krissinel and K. Henrick (*86*)] for the representative structure of the ensemble.

asymmetric reverse-protonation of the complex components and exploits the sensitivity of 2D homonuclear NOESY experiments.

A major limitation in using the 2D approaches mentioned above for studying intermolecular interactions is the assignment of the observed intermolecular interactions to the corresponding protons in the complex constituents. In the past, the assignment had to rely on modeling the complex structure and the availability of biochemical data on the binding interface combined with specific amino acid labeling. In this study, we demonstrate that the analysis of the intermolecular interactions can be considerably aided by the sequential and side chain assignment procedures recently developed by Yang and co-workers (*55*, *56*). Nevertheless, the assignment of some intermolecular interactions still had to rely on preliminary models and labeling schemes.

As demonstrated in this study, the section of the NOESY spectrum showing interactions between aromatic protons and aliphatic protons with resonances upfield of 2.5 ppm can be simplified to show almost exclusively cross-peaks due to intermolecular interactions. Despite the simplification of the spectra, some contributions from amide protons that resisted exchange with D_2O have been observed. In addition, some cross-peaks due to less than 100% deuteration of the commercial growth medium and/or scrambling have been observed. Most of these contributions can be identified via measurement of the NOESY spectra of the free proteins.

In summary, 24 new intermolecular NOEs were identified using the reverse-labeling method developed in this study. These NOEs were introduced as distance restraints into a docking calculation of the IFNAR2−IFNα2 complex which yielded a considerably improved model revealing new information about the structure of the binding interface.

Comparison with Previously Calculated Docking Models of the IFNAR2−IFNα2 Complex. Inclusion of a much larger number of intermolecular NOEs substantially improved the quality of the model for the IFNAR2−IFNα2 complex and increased the surface of the binding site by approximately 2-fold for both molecules compared with those in previous models (Table 3). The high quality of the new model is also evident from the substantial increase in the number of possible hydrogen bonds and salt bridges in comparison to the numbers in the

Table 4: Intermolecular Salt Bridges and Hydrogen Bonds Formed in the Docking Model of the IFNAR2−IFNα2 Complex[a]

	IFNα2		IFNAR2	
	residue	atom	residue	atom
hydrogen bonds	T6	O	K48	NZ
	R12	NH2	D138	OD2
	R12	NH1	H187	O
	R13	NH2	S188	O
	R22	NH1	N98	OD1
	D35	OD1	K48	NZ
	E146	OE1	S47	OG
	E146	OE2	K48	NZ
	R149	NE	E77	OE2
	N156	OD1	Q136	NE2
	R162	NH1	D70	OD1
	R162	NH1	D70	OD1
salt bridges	R12	NH1	D138	OD2
	R12	NH2	D138	OD2
	R33	NH1	E50	OE1
	D35	OD1	K48	NZ
	E146	OE1	K48	NZ
	E146	OE2	K48	NZ
	R149	NE	E77	OE2
	R149	NH2	E77	OE2
	E159	OE1	H76	NE2
	R162	NH1	D70	OD1
	R162	NH2	D70	OD1

[a]Intermolecular contacts were calculated using PISA [protein interfaces, surfaces, and assembly service at the European Bioinformatics Institute, authored by E. Krissinel and K. Henrick (*86*)] and are reported if present in at least five of the 10 structures in the ensemble.

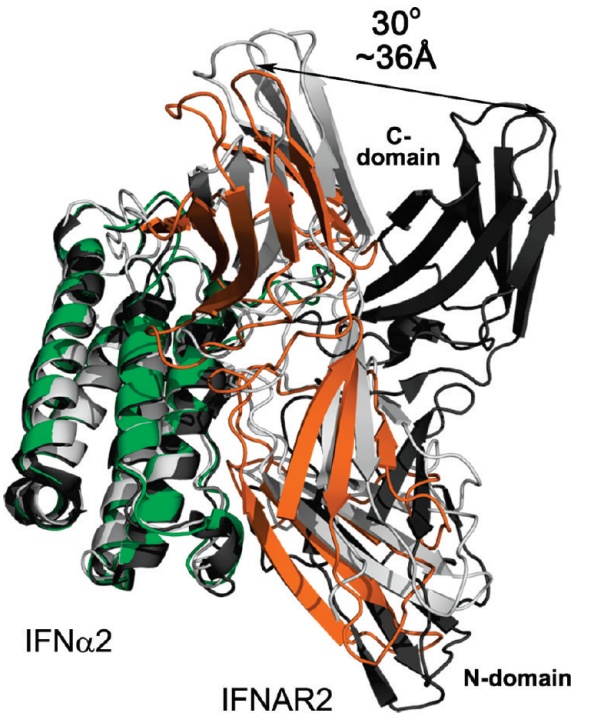

FIGURE 8: New and previous docking models of the IFNAR2−IFNα2 complex, with a change in the orientation of IFNAR2 relative to IFNα2. Representative structures of our model (IFNα2 colored green and IFNAR2 orange), the model of Quadt-Akabayov et al. (*26*) (dark gray), and the model of Chill et al. (*18*) (light gray) are aligned with respect to IFNα2. The flexible N-terminal (^{R2}S1−^{R2}C12) and C-terminal residues (^{R2}P204− ^{R2}S212) of IFNAR2 were removed from the new model and that of Quadt-Akabayov et al. (*26*).

models of Chill et al. and Quadt-Akabayov et al. (Table 3) (*18*, *26*). Our study reveals a second large surface in the binding site of the two molecules that is made of a mosaic of positively and negatively charged residues as well as some polar residues. The contribution of hydrophobic residues to this section is very minor.

The NOE constraints used in the docking are well-dispersed over the entire binding surface, connecting most of the various determinants situated in the binding site [A helix, A−B loop, and E helix in IFNα2 as well as S3−S4, S5−S6, S7−S8, and S13−S14 loops in IFNAR2 (see Figures 6 and 7 and Figure 2S of the Supporting Information)]. The N-terminus and A helix of IFNα2 were not found to be a part of the binding site in the NMR mapping done by Quadt-Akabayov et al. since cross-peaks belonging to the amide pairs of these residues were missing in the cross-saturation ^{15}N HSQC spectrum of bound IFNα2 (*26*). These cross-peaks were not observed because of the low sample concentration and a further 10-fold reduction in the amide cross-peak intensity caused by the use of a 10% H_2O/90% D_2O solution required to prevent spin diffusion (*26*). The four DMC restraints and the single NOE used in the calculation of the Quadt-Akabayov et al. docking model connected only a subset of regions found to be involved in binding by previous mutagenesis and NMR studies (*22*, *23*, *25*) (Table 1). This subset also did not include the A helix of IFNα2. All of the above resulted in exclusion of the A helix of IFNα2 from the interface and a 30° difference in the orientation of IFNAR2 relative to IFNα2 in comparison with the new model (Figure 8). Chill et al. used the same four DMC restraints in the docking of their model that were used by Quadt-Akabayov et al. However, because of the lack of experimental data, no emphasis on a binding interface that excludes the A helix was imposed in the calculation (*18*), resulting in incorporation of the A helix in the interface and orientation of IFNAR2 relative to IFNα2 much closer to that found in this study (Figures 6 and 8). The input data for the docking model presented in this study consisted of the same binding site mapping and distance restraints used for the calculation of the Quadt-Akabayov et al. model with the addition of the 24 new NOEs found in this work. Therefore, in view of the limitations of binding site mapping techniques, we can conclude that the incorporation of a high number of experimental intermolecular distance constraints well dispersed over most of the binding site surface is essential for the calculation of a docking model which reveals the entire binding interface and the correct orientation of complex components.

An attempt was made to incorporate residual dipolar couplings (RDCs) in the structure calculation. Several alignment media were tested for the measurement of RDCs of the IFNAR2−/IFNα2 complex, and most of these were found not to be suitable. The sample was stable in a polyacrylamide gel doped with negative charges (*97*); however, the relevant spectra exhibited a low S/N, which allowed us to obtain only a small number of RDCs. Most of these RDCs were for residues situated in flexible regions making their contribution to structure calculation very limited (*98*).

Structural analysis of the models of Chill et al. and Quadt-Akabayov et al. shows that the regions of IFNα2 and IFNAR2 added to the binding surface were not far apart in the previous models. Inclusion of a high number of intermolecular NOEs in the new model brings the two proteins much closer together, revealing the participation of the regions described above in the binding interface.

The significant increase in the binding area on IFNα2 is mostly attributed to the addition of the N-terminus, A helix, and part of the C-terminus (Figures 6 and 7). While the A helix is connected with IFNAR2 by 12 intermolecular NOEs (Table 1 and Figure 7) ($^{\alpha2}$L15−^{R2}W100, $^{\alpha2}$L15−^{R2}H76, $^{\alpha2}$R12−^{R2}H76, and $^{\alpha2}$R12−^{R2}H187), NOEs involving the N-terminal and C-terminal residues of IFNα2 ($^{\alpha2}$Q5, $^{\alpha2}$T6, $^{\alpha2}$H7, $^{\alpha2}$L9, $^{\alpha2}$E159, $^{\alpha2}$L161, $^{\alpha2}$R162, $^{\alpha2}$S163, and $^{\alpha2}$K164) were not detected since mostly these interactions do not involve aromatic−aliphatic proton interactions. Six of these nine residues were not found to participate in IFNAR2 binding by the NMR cross-saturation studies because of the lack of information: the HN resonances of four are unassigned ($^{\alpha2}$T6, $^{\alpha2}$H7, $^{\alpha2}$L9, and $^{\alpha2}$S163) and the HN cross-peaks of the remaining two ($^{\alpha2}$Q5 and $^{\alpha2}$L161) were missing from the cross-saturation ^{15}N HSQC spectrum of the bound IFNα2 because of their low intensity as mentioned in the previous paragraphs (*26*). The remaining three residues ($^{\alpha2}$E159, $^{\alpha2}$R162, and $^{\alpha2}$K164) did not show a significant decrease in their HN cross-peak intensity upon IFNAR2 binding. However, residues from the C-terminus of IFNα2 ($^{\alpha2}$R162 and $^{\alpha2}$E165) were found to be part of the binding site in the Quadt-Akabayov et al. docking model (Figure 6), while residues $^{\alpha2}$E159 and $^{\alpha2}$L161 are situated less than 8 Å from IFNAR2. Residues 5−9 from the C-terminal tail of IFNα2 are less than 14 Å from IFNAR2 because of the more distant position of the N-terminal part of IFNα2 from IFNAR2 in the Quadt-Akabayov et al. model (*26*). In the Chill et al. model, the entire C-terminal tail of IFNα2 (residues 157−165) was excluded from the calculation because of difficulties in docking such a flexible segment (Figure 6) (*18*). Residues $^{\alpha2}$T6, $^{\alpha2}$H7, and $^{\alpha2}$L9 as well as residue $^{\alpha2}$Q5 from the N-terminal tail of IFNα2 are situated less than 5 and 8 Å from IFNAR2, respectively, in the Chill et al. model (*18*). It is important to point out that the N-terminal tail of IFNα2 features a disulfide bond connecting the first N-terminal cysteine with another cysteine in the C-helix (C98). As a result of the formation of this covalent bond, the mobility of the N-terminus of IFNα2 is restricted as manifested by a positive H−N NOE in the range of 0.4−0.6 in comparison with the negative NOEs measured for the flexible C-terminus (*15*). Moreover, three residues in the N-terminus of IFNα2 ($^{\alpha2}$C1, $^{\alpha2}$L3, and $^{\alpha2}$L9) are absolutely conserved among 35 IFNα species (*15*), suggesting the possible involvement of the latter two in IFNAR2 or IFNAR1 binding.

The binding site on IFNAR2 has grown compared to those of the previous models mostly because of the addition of charged or polar residues from the C domain of the protein. One intermolecular NOE connects the S13−S14 loop of the C domain of IFNAR2 with IFNα2 ($^{\alpha2}$R12−^{R2}H187), confirming the participation of this domain in the binding interface (Table 1 and Figure 7). Residue ^{R2}L139 displays a change in the chemical shift of one of its methyl groups as seen in Figure 3, placing it and its direct neighbors (^{R2}S140 and ^{R2}D138) in the binding site. However, all the other residues in the C domain of IFNAR2 revealed by the new model as a part of the interface (^{R2}E132−^{R2}Q136 and ^{R2}K159) are not connected by NOEs to IFNα2 and do not show any change in the position of their HN cross-peaks upon IFNα2 binding (*19*). Several of these residues have been suggested by mutagenesis studies to be involved in IFNα2 binding (*24*) as will be elaborated in the following section. In the Quadt-Akabayov et al. model, residues 138−140, 159, 186, and 187 from the C domain of IFNAR2 were found to be part of the interface (Figure 6) while residues 132−137 are situated less than 8 Å from IFNα2 (*26*). Analysis of the intermolecular distances in the Chill et al. model (*18*) shows that residues 136−140, 159, and 186−189 are situated less than 4.5 Å from the interfacial residues of IFNα2. In addition, a significant attenuation of the signal was observed in the HN cross-peaks of residues in the S13−S14 loop of the C domain of IFNAR2 (residues 187−198) upon IFNα2 binding.

In summary, the new model adds to the binding surface residues from both IFNAR2 and IFNα2 which were not shown by previous NMR mapping studies to be affected by binding. Previous mapping of the binding sites was performed by examination of changes in the position or intensity of the HN cross-peaks in the ^{15}N HSQC spectra of bound IFNAR2 and IFNα2 (*18*, *26*). However, NMR experiments showing backbone resonances are in most cases unable to detect changes in cross-peaks of residues participating in the binding through their side chain and not backbone atoms. Therefore, we believe that residues not found to be in the interface by ^{15}N HSQC type NMR mapping could still be a part of the binding surface provided they interact through their side chains, which is very probable in the case of the charged and polar residues such as the ones added to the interface in the new model. It is important to mention that NOE is the most reliable and informative NMR parameter for gaining intermolecular structural information. Therefore, we believe that the 24 NOEs incorporated into the docking of the new model, being well dispersed over the binding surface, serve as anchoring points for the entire set of interface contacts, including areas not directly connected by NOEs. The participation of these new regions in the binding site is an immediate consequence of the input of these NOE distance constraints into the docking calculation.

To assess the robustness of the model determined by the large number of intermolecular NOE constraints, we performed a HADDOCK run with the newly found intermolecular NOEs only. The two models were very similar in terms of rmsd (backbone and heavy atom rmsd's of 1.07 and 1.21 Å, respectively). However, the energetic parameters of the docking calculation were significantly improved with the inclusion of the DMC and previously obtained single-NOE restraints. Another docking calculation was performed using only ∼70% of the intermolecular NOEs found in this study. In this calculation, NOEs between ^{R2}L52 and $^{\alpha2}$F27, ^{R2}H76 and $^{\alpha2}$L15, ^{R2}H76 and $^{\alpha2}$R12, and ^{R2}H187 and $^{\alpha2}$R12 as well as the single NOE obtained previously by Quadt-Akabayov et al. (*26*) were removed from the distance restraint list; however, the DMC distance restraints were kept (Figure 2S of the Supporting Information). The resulting model was also very similar to the model containing all the distance restraints both in terms of the overall rmsd and in terms of the relative orientation between IFNAR2 and IFNα2 (backbone and heavy atom rmsd's of 1.53 and 1.66 Å, respectively), further supporting the robustness of the proposed model and the correct assignment of the intermolecular NOEs used to obtain it.

Comparison with the Mutagenesis Data of the IFNAR2−IFNα2 Complex. The individual binding sites on IFNAR2 and IFNα2, as determined by our docking model, are in good agreement with the mutational data available (Figure 7). Residues found by mutagenesis to be important for IFNAR2−IFNα2 binding form a subset of the interface residues found in the new model. It is important to point out that IFNα2 residues $^{\alpha2}$R12 and $^{\alpha2}$L15 from the A helix and $^{\alpha2}$L153 from the E helix, which were not found by previous NMR studies to participate in the binding due to a lack of assignment, were found in this study to give rise to intermolecular NOEs. These residues were found by mutagenesis studies to have a significant effect on the binding

of IFNα2 to IFNAR2, strongly supporting the intermolecular NOEs obtained for them.

Several regions in the interface of the new model were not subjected to mutational analysis or did not have a pronounced effect on binding affinity upon mutation. On IFNα2, these areas include the N- and C-termini, the first of which was not studied by mutagenesis, while the latter might participate in binding as can be concluded from the 2-fold decrease in the binding affinity upon removal of five C-terminal residues ($^{\alpha 2}$L161−$^{\alpha 2}$E165) (*23*, *24*). The contribution of the C domain of IFNAR2 to the binding has been thought to be small, mainly since mutagenesis studies revealed minor effects on the binding affinity of IFNAR2 for IFNα2 upon mutation of C-terminal domain residues or removal of the entire C domain of IFNAR2 (*99*). However, in this study, two NOEs are connecting the S13−S14 loop of IFNAR2 (specifically ^{R2}H187) with the A helix of IFNα2, demonstrating a clear involvement of the C domain in the binding site. In addition, the previously mentioned chemical shift change in the resonance of a methyl group of ^{R2}L139 further supports the participation of this domain in the binding interface. Areas from the C domain of IFNAR2 are situated very close to the binding interface in all the docking models of the IFNAR2−IFNα2 complex obtained over the years, beginning with the model calculated by Roisman et al. and ending with the current model (*18*, *25*, *26*). Single mutations of residues ^{R2}E132, ^{R2}E133, ^{R2}E134, and ^{R2}Q136 as well as multiple alanine substitutions in the S11−S12 loop of IFNAR2 (^{R2}E157-IKG-N161 to ^{157}AIAGN^{161}) had a very minor effect on binding affinity (*20*, *22*). However, a triple alanine substitution of ^{R2}E132−^{R2}E134 decreased binding affinity 2-fold (*24*). In addition, recently, an interaction between the IFN C-terminus and a negatively charged loop in the IFNAR2 C domain (^{R2}E132−^{R2}E134) has been suggested to play a role in the differential signaling of the various type I IFNs by causing an up to 20-fold difference in binding affinities for IFNAR2 upon insertion of C-terminal tails from different αIFNs into an IFNα2 scaffold (*24*). Slutzky et al. docked the C-terminal tail of the IFNα2 mutant containing the IFNα8 C-terminal tail and found it to gain a specific structure in the bound state, binding to a groove below the ^{R2}E132−^{R2}E134 loop in IFNAR2 (*24*). On the basis of this study, it is plausible to suggest that the entropic cost of ordering the unstructured C-terminal tail of IFNα2 upon binding could cause an only small and insignificant change in ΔG upon complex formation for mutants preventing this interaction (such as those lacking the C tail of IFNα2 and/or a negative charge in the ^{R2}E132−^{R2}E134 loop of IFNAR2). It has been shown previously for the complex between the human growth hormone and its receptor that while two-thirds of the interface residues had little impact on the binding affinity, large and compensating changes were observed in the enthalpy and entropy of binding (*100*). This study further supports the claim that residues not found to have an effect on binding kinetics or affinity can still be part of a binding interface (*100*).

Allostery in the Binding of IFNAR1-EC to the IFNα2−IFNAR2 Complex. Recently, we found that binding of IFNAR1-EC to the IFNα2−IFNAR2 complex resulted in the significant chemical shift changes or disappearance of HSQC cross-peaks of residues on the face of IFNα2 containing the binding site for IFNAR2 (*101*). However, only three of these residues ($^{\alpha 2}$F27, $^{\alpha 2}$R149, and $^{\alpha 2}$S152) were implicated in IFNAR2 binding by NMR cross-saturation studies (*26*). As shown in Figure 9, this study demonstrates that residues $^{\alpha 2}$Q5, $^{\alpha 2}$N156, $^{\alpha 2}$E159, $^{\alpha 2}$S160, and $^{\alpha 2}$K164, whose HSQC cross-peaks disappeared upon IFNAR1 binding, are located in IFNα2 binding site for IFNAR2. Moreover, $^{\alpha 2}$Q20 and $^{\alpha 2}$R22 which changed their chemical shift upon IFNAR1 binding are also in the binding site for IFNAR2 in our model. Thus, the model presented here more than doubles the number of IFNα2 residues in the binding site for IFNAR2 whose HSQC cross-peaks were affected by IFNAR1 binding, strongly supporting the proposed allosteric changes in the IFNα2−IFNAR2 complex upon IFNAR1 binding. Unfortunately, the exact structural nature of this allostery is not known since the atomic-resolution structure of the ternary IFNAR1−IFNα2−IFNAR2 complex has not been elucidated thus far.

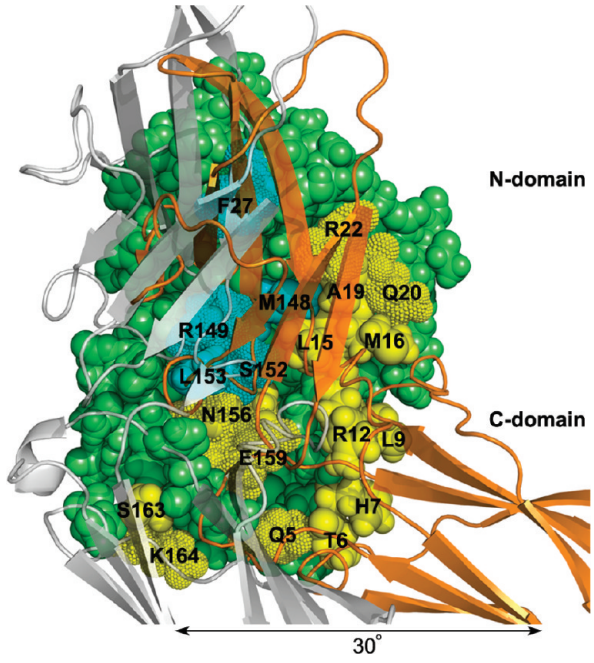

FIGURE 9: Effect of binding of IFNAR1-EC to the binary IFNAR2−IFNα2 complex on IFNα2 binding site. Representative structures of our model and that of Quadt-Akabayov et al. (*26*) are aligned with respect to IFNα2. IFNα2 is shown as a light green space-filling representation, while IFNAR2 from our model or that of Quadt-Akabayov et al. (*26*) is represented by an orange or light gray ribbon diagram, respectively. The flexible N-terminal (^{R2}S1−^{R2}C12) and C-terminal (^{R2}P204−^{R2}S212) residues of IFNAR2 were removed from the new model and that of Quadt-Akabayov et al. (*26*). Residues colored cyan or yellow are IFNα2 binding site residues for IFNAR2, excluding those unaffected by binding of IFNAR1 to the IFNα2−IFNAR2 complex (*101*). Residues that exhibited a significant change in chemical shift or could not be assigned due to large chemical shift changes or the disappearance upon IFNAR1 binding are dotted. All the other colored residues could not be assigned because of overlap or a lack of assignment in the binary complex (*101*). Residues situated in the binding interface of the previous model are colored cyan (*26*). Residues added to the interface by the current model are colored yellow.

Conclusions. In this study, we present a novel approach for obtaining intermolecular side chain−side chain NOEs in large protein complexes using asymmetric reverse-protonation and 2D homonuclear NOESY spectra. Applying this technique to the 44 kDa IFNα2−IFNAR2 complex yielded 24 new intermolecular NOEs which were used as distance restraints in the docking calculation of a model of the complex. This model doubles the binding site surface on both IFNα2 and IFNAR2 by adding a new section in the lower part of IFNα2 and IFNAR2 binding sites that is formed by a mosaic of charged and polar residues. A significant 30° change was observed in the orientation of IFNAR2 relative to IFNα2 in comparison with the Quadt-Akabayov et al. model (*26*)

as a result of the addition of the newly found intermolecular NOEs which makes it much more similar to the model previously suggested by Chill et al. (*18*). Moreover, this study demonstrates that practically the entire IFNα2 binding site for IFNAR2 undergoes conformational changes upon IFNAR1 binding, strongly supporting a mechanism of allosteric changes in IFNα2 caused by binding of IFNAR1 to the IFNα2−IFNAR2 complex.

ACKNOWLEDGMENT

We are most grateful to Dr. Naama Kessler for help with protein expression and purification. We also thank Dr. Lewis Kay, Dr. Tali Scherf, Dr. Osnat Rosen, and Dr. Jordan Chill for helpful suggestions and discussions.

SUPPORTING INFORMATION AVAILABLE

Figure showing the elimination of very slowly exchanging amide protons from the 2D NOESY spectra of asymmetrically labeled IFNAR2−IFNα2 complexes and figure showing the open book representation of the IFNAR2-IFNα2 complex with the NOE/DMC interactions used in the docking calculation. This material is available free of charge via the Internet at http://pubs.acs.org.

REFERENCES

1. Kirkwood, J. (2002) Cancer immunotherapy: The interferon-α experience. *Semin. Oncol. 29*, 18–26.
2. Perry, C. M., and Jarvis, B. (2001) Peginterferon-α-2a (40 kD): A review of its use in the management of chronic hepatitis C. *Drugs 61*, 2263–2288.
3. Pestka, S., Krause, C. D., and Walter, M. R. (2004) Interferons, interferon-like cytokines, and their receptors. *Immunol. Rev. 202*, 8–32.
4. Biron, C. A. (2001) Interferons α and *β* as immune regulators: A new look. *Immunity 14*, 661–664.
5. Stark, G. R., Kerr, I. M., Williams, B. R. G., Silverman, R. H., and Schreiber, R. D. (1998) How Cells Respond to Interferons. *Annu. Rev. Biochem. 67*, 227–264.
6. Novick, D., Cohen, B., and Rubinstein, M. (1994) The human interferon α/*β* receptor: Characterization and molecular cloning. *Cell 77*, 391–400.
7. Uze, G., Lutfalla, G., and Mogensen, K. E. (1995) α and *β* interferons and their receptor and their friends and relations. *J. Interferon Cytokine Res. 15*, 3–26.
8. de Weerd, N. A., Samarajiwa, S. A., and Hertzog, P. J. (2007) Type I interferon receptors: Biochemistry and biological functions. *J. Biol. Chem. 282*, 20053–20057.
9. Ozbek, S., Grotzinger, J., Krebs, B., Fischer, M., Wollmer, A., Jostock, T., Mullberg, J., and Rose-John, S. (1998) The membrane proximal cytokine receptor domain of the human interleukin-6 receptor is sufficient for ligand binding but not for gp130 association. *J. Biol. Chem. 273*, 21374–21379.
10. Cunningham, B. C., Ultsch, M., De Vos, A. M., Mulkerrin, M. G., Clauser, K. R., and Wells, J. A. (1991) Dimerization of the extracellular domain of the human growth hormone receptor by a single hormone molecule. *Science 254*, 821–825.
11. Gent, J., Van Den Eijnden, M., Van Kerkhof, P., and Strous, G. J. (2003) Dimerization and signal transduction of the growth hormone receptor. *Mol. Endocrinol. 17*, 967–975.
12. Krause, C. D., and Pestka, S. (2005) Evolution of the class 2 cytokines and receptors, and discovery of new friends and relatives. *Pharmacol. Ther. 106*, 299–346.
13. Bernat, B., Pal, G., Sun, M., and Kossiakoff, A. A. (2003) Determination of the energetics governing the regulatory step in growth hormone-induced receptor homodimerization. *Proc. Natl. Acad. Sci. U.S.A. 100*, 952–957.
14. Remy, I., Wilson, I. A., and Michnick, S. W. (1999) Erythropoietin receptor activation by a ligand-induced conformation change. *Science 283*, 990–993.
15. Klaus, W., Gsell, B., Labhardt, A. M., Wipf, B., and Senn, H. (1997) The three-dimensional high resolution structure of human interferon α-2a determined by heteronuclear NMR spectroscopy in solution. *J. Mol. Biol. 274*, 661–675.
16. Karpusas, M., Nolte, M., Benton, C. B., Meier, W., Lipscomb, W. N., and Goelz, S. (1997) The crystal structure of human interferon *β* at 2.2-Å resolution. *Proc. Natl. Acad. Sci. U.S.A. 94*, 11813–11818.
17. Radhakrishnan, R., Walter, L. J., Hruza, A., Reichert, P., Trotta, P. P., Nagabhushan, T. L., and Walter, M. R. (1996) Zinc mediated dimer of human interferon-α 2b revealed by X-ray crystallography. *Structure 4*, 1453–1463.
18. Chill, J. H., Quadt, S. R., Levy, R., Schreiber, G., and Anglister, J. (2003) The human type I interferon receptor: NMR structure reveals the molecular basis of ligand binding. *Structure 11*, 791–802.
19. Chill, J. H., Nivasch, R., Levy, R., Albeck, S., Schreiber, G., and Anglister, J. (2002) The human interferon receptor: NMR-based modeling, mapping of the IFN-α2 binding site, and observed ligand-induced tightening. *Biochemistry 41*, 3575–3585.
20. Chuntharapai, A., Gibbs, V., Lu, J., Ow, A., Marsters, S., Ashkenazi, A., De Vos, A., and Jin Kim, K. (1999) Determination of residues involved in ligand binding and signal transmission in the human IFN-α receptor 2. *J. Immunol. 163*, 766–773.
21. Lewerenz, M., Mogensen, K. E., and Uze, G. (1998) Shared receptor components but distinct complexes for α and *β* interferons. *J. Mol. Biol. 282*, 585–599.
22. Piehler, J., and Schreiber, G. (1999) Mutational and structural analysis of the binding interface between type I interferons and their receptor Ifnar2. *J. Mol. Biol. 294*, 223–237.
23. Piehler, J., Roisman, L. C., and Schreiber, G. (2000) New structural and functional aspects of the type I interferon-receptor interaction revealed by comprehensive mutational analysis of the binding interface. *J. Biol. Chem. 275*, 40425–40433.
24. Slutzki, M., Jaitin, D. A., Yehezkel, T. B., and Schreiber, G. (2006) Variations in the unstructured C-terminal tail of interferons contribute to differential receptor binding and biological activity. *J. Mol. Biol. 360*, 1019–1030.
25. Roisman, L. C., Piehler, J., Trosset, J. Y., Scheraga, H. A., and Schreiber, G. (2001) Structure of the interferon-receptor complex determined by distance constraints from double-mutant cycles and flexible docking. *Proc. Natl. Acad. Sci. U.S.A. 98*, 13231–13236.
26. Quadt-Akabayov, S. R., Chill, J. H., Levy, R., Kessler, N., and Anglister, J. (2006) Determination of the human type I interferon receptor binding site on human interferon-α2 by cross saturation and an NMR-based model of the complex. *Protein Sci. 15*, 2656–2668.
27. Clore, G. M., and Gronenborn, A. M. (1997) NMR structures of proteins and protein complexes beyond 20,000 M(r). *Nat. Struct. Biol. 4* (Suppl.), 849–853.
28. Grzesiek, S., Anglister, J., Ren, H., and Bax, A. (1993) Carbon-13 line narrowing by deuterium decoupling in deuterium/carbon-13/nitrogen-15 enriched proteins. Application to triple resonance 4D J connectivity of sequential amides. *J. Am. Chem. Soc. 115*, 4369–4370.
29. Sattler, M., and Fesik, S. W. (1996) Use of deuterium labeling in NMR: Overcoming a sizeable problem. *Structure 4*, 1245–1249.
30. Pervushin, K., Riek, R., Wider, G., and Wuthrich, K. (1997) Attenuated T2 relaxation by mutual cancellation of dipole-dipole coupling and chemical shift anisotropy indicates an avenue to NMR structures of very large biological macromolecules in solution. *Proc. Natl. Acad. Sci. U.S.A. 94*, 12366–12371.
31. Kay, L. E. (2005) NMR studies of protein structure and dynamics. *J. Magn. Reson. 173*, 193–207.
32. Tugarinov, V., Hwang, P. M., and Kay, L. E. (2004) Nuclear magnetic resonance spectroscopy of high-molecular-weight proteins. *Annu. Rev. Biochem. 73*, 107–146.
33. Smith, B. O., Ito, Y., Raine, A., Teichmann, S., BenTovim, L., Nietlispach, D., Broadhurst, R. W., Terada, T., Kelly, M., Oschkinat, H., Shibata, T., Yokoyama, S., and Laue, E. D. (1996) An approach to global fold determination using limited NMR data from larger proteins selectively protonated at specific residue types. *J. Biomol. NMR 8*, 360–368.
34. Kelly, M. J. S., Krieger, C., Ball, L. J., Yu, Y. H., Richter, G., Schmieder, P., Bacher, A., and Oschkinat, H. (1999) Application of amino acid type-specific H-1- and N-14-labeling in a H-2-, N-15-labeled background to a 47 kDa homodimer: Potential for NMR structure determination of large proteins. *J. Biomol. NMR 14*, 79–83.
35. Kelly, M. J. S., Ball, L. J., Krieger, C., Yu, Y. H., Fischer, M., Schiffmann, S., Schmieder, P., Kuhne, R., Bermel, W., Bacher, A., Richter, G., and Oschkinat, H. (2001) The NMR structure of the 47-kDa dimeric enzyme 3,4-dihydroxy-2-butanone-4-phosphate synthase and ligand binding studies reveal the location of the active site. *Proc. Natl. Acad. Sci. U.S.A. 98*, 13025–13030.

36. Arrowsmith, C. H., Pachter, R., Altman, R. B., Iyer, S. B., and Jardetzky, O. (1990) Sequence-Specific H-1-Nmr Assignments and Secondary Structure in Solution of *Escherichia coli* Trp Repressor. *Biochemistry 29*, 6332–6341.
37. Arrowsmith, C., Pachter, R., Altman, R., and Jardetzky, O. (1991) The Solution Structures of *Escherichia coli* Trp Repressor and Trp Aporepressor at an Intermediate Resolution. *Eur. J. Biochem. 202*, 53–66.
38. Aghazadeh, B., Zhu, K., Kubiseski, T. J., Liu, G. A., Pawson, T., Zheng, Y., and Rosen, M. K. (1998) Structure and mutagenesis of the Dbl homology domain. *Nat. Struct. Biol. 5*, 1098–1107.
39. Medek, A., Olejniczak, E. T., Meadows, R. P., and Fesik, S. W. (2000) An approach for high-throughput structure determination of proteins by NMR spectroscopy. *J. Biomol. NMR 18*, 229–238.
40. Ito, T., Marintchev, A., and Wagner, G. (2004) Solution structure of human initiation factor eIF2α reveals homology to the elongation factor eEF1B. *Structure 12*, 1693–1704.
41. Yu, L. P., Sun, C. H., Song, D. Y., Shen, J. W., Xu, N., Gunasekera, A., Hajduk, P. J., and Olejniczak, E. T. (2005) Nuclear magnetic resonance structural studies of a potassium channel-charybdotoxin complex. *Biochemistry 44*, 15834–15841.
42. Frueh, D. P., Arthanari, H., Koglin, A., Vosburg, D. A., Bennett, A. E., Walsh, C. T., and Wagner, G. (2008) Dynamic thiolation-thioesterase structure of a non-ribosomal peptide synthetase. *Nature 454*, 903–906.
43. Gardner, K. H., Rosen, M. K., and Kay, L. E. (1997) Global folds of highly deuterated, methyl-protonated proteins by multidimensional NMR. *Biochemistry 36*, 1389–1401.
44. Rosen, M. K., Gardner, K. H., Willis, R. C., Parris, W. E., Pawson, T., and Kay, L. E. (1996) Selective methyl group protonation of perdeuterated proteins. *J. Mol. Biol. 263*, 627–636.
45. Tugarinov, V., Choy, W.-Y., Orekhov, V. Y., and Kay, L. E. (2005) Solution NMR-derived global fold of a monomeric 82-kDa enzyme. *Proc. Natl. Acad. Sci. U.S.A. 102*, 622–627.
46. Gross, J. D., Moerke, N. J., von der Haar, T., Lugovskoy, A. A., Sachs, A. B., McCarthy, J. E., and Wagner, G. (2003) Ribosome loading onto the mRNA cap is driven by conformational coupling between eIF4G and eIF4E. *Cell 115*, 739–750.
47. Garrett, D. S., Seok, Y. J., Peterkofsky, A., Gronenborn, A. M., and Clore, G. M. (1999) Solution structure of the 40,000 Mr phosphoryl transfer complex between the N-terminal domain of enzyme I and HPr. *Nat. Struct. Biol. 6*, 166–173.
48. Van Horn, W. D., Kim, H. J., Ellis, C. D., Hadziselimovic, A., Sulistijo, E. S., Karra, M. D., Tian, C. L., Sonnichsen, F. D., and Sanders, C. R. (2009) Solution Nuclear Magnetic Resonance Structure of Membrane-Integral Diacylglycerol Kinase. *Science 324*, 1726–1729.
49. Suzuki, M., Lee, D. Y., Inyamah, N., Stadtman, T. C., and Tjandra, N. (2008) Solution NMR structure of selenium-binding protein from *Methanococcus vannielii*. *J. Biol. Chem. 283*, 25936–25943.
50. Parsons, L., Bonander, N., Eisenstein, E., Gilson, M., Kairys, V., and Orban, J. (2003) Solution structure and functional ligand screening of HI0719, a highly conserved protein from bacteria to humans in the YjgF/YER057c/UK114 family. *Biochemistry 42*, 80–89.
51. Caffrey, M., Cai, M. L., Kaufman, J., Stahl, S. J., Wingfield, P. T., Covell, D. G., Gronenborn, A. M., and Clore, G. M. (1998) Three-dimensional solution structure of the 44 kDa ectodomain of SIV gp41. *EMBO J. 17*, 4572–4584.
52. Ma, D. J., Tillman, T. S., Tang, P., Meirovitch, E., Eckenhoff, R., Carnini, A., and Xu, Y. (2008) NMR studies of a channel protein without membranes: Structure and dynamics of water-solubilized KcsA. *Proc. Natl. Acad. Sci. U.S.A. 105*, 16537–16542.
53. Popovych, N., Tzeng, S. R., Tonelli, M., Ebright, R. H., and Kalodimos, C. G. (2009) Structural basis for cAMP-mediated allosteric control of the catabolite activator protein. *Proc. Natl. Acad. Sci. U.S.A. 106*, 6927–6932.
54. Hong, E., Lee, H. M., Ko, H., Kim, D. U., Jeon, B. Y., Jung, J., Shin, J., Lee, S. A., Kim, Y., Jeon, Y. H., Cheong, C., Cho, H. S., and Lee, W. (2007) Structure of an atypical orphan response regulator protein supports a new phosphorylation-independent regulatory mechanism. *J. Biol. Chem. 282*, 20667–20675.
55. Xu, Y., Zheng, Y., Fan, J. S., and Yang, D. (2006) A new strategy for structure determination of large proteins in solution without deuteration. *Nat. Methods 3*, 931–937.
56. Xu, Y., Lin, Z., Ho, C., and Yang, D. (2005) A general strategy for the assignment of aliphatic side-chain resonances of uniformly ^{13}C,^{15}N-labeled large proteins. *J. Am. Chem. Soc. 127*, 11920–11921.
57. Otting, G., and Wuthrich, K. (1990) Heteronuclear Filters in 2-Dimensional [H-1, H-1] Nmr-Spectroscopy: Combined Use with Isotope Labeling for Studies of Macromolecular Conformation and Intermolecular Interactions. *Q. Rev. Biophys. 23*, 39–96.
58. Otting, G., and Wuthrich, K. (1988) Efficient Purging Scheme for Proton-Detected Heteronuclear Two-Dimensional Nmr. *J. Magn. Reson. 76*, 569–574.
59. Ikura, M., and Bax, A. (1992) Isotope-Filtered 2d Nmr of a Protein Peptide Complex: Study of a Skeletal-Muscle Myosin Light Chain Kinase Fragment Bound to Calmodulin. *J. Am. Chem. Soc. 114*, 2433–2440.
60. Kogler, H., Sorensen, O. W., Bodenhausen, G., and Ernst, R. R. (1983) Low-Pass J-Filters: Suppression of Neighbor Peaks in Heteronuclear Relayed Correlation Spectra. *J. Magn. Reson. 55*, 157–163.
61. Breeze, A. L. (2000) Isotope-filtered NMR methods for the study of biomolecular structure and interactions. *Prog. Nucl. Magn. Res. 36*, 323–372.
62. Koglin, A., Lohr, F., Bernhard, F., Rogov, V. V., Frueh, D. P., Strieter, E. R., Mofid, M. R., Guntert, P., Wagner, G., Walsh, C. T., Marahiel, M. A., and Dotsch, V. (2008) Structural basis for the selectivity of the external thioesterase of the surfactin synthetase. *Nature 454*, 907–911.
63. Takeuchi, K., Roehrl, M. H. A., Sun, Z. Y. J., and Wagner, G. (2007) Structure of the calcineurin-NFAT complex: Defining a T cell activation switch using solution NMR and crystal coordinates. *Structure 15*, 587–597.
64. Gross, J. D., Gelev, V. M., and Wagner, G. (2003) A sensitive and robust method for obtaining intermolecular NOEs between side chains in large protein complexes. *J. Biomol. NMR 25*, 235–242.
65. Piehler, J., and Schreiber, G. (1999) Biophysical analysis of the interaction of human ifnar2 expressed in *E. coli* with IFNα2. *J. Mol. Biol. 289*, 57–67.
66. Delaglio, F., Grzesiek, S., Vuister, G. W., Zhu, G., Pfeifer, J., and Bax, A. (1995) Nmrpipe: A Multidimensional Spectral Processing System Based on Unix Pipes. *J. Biomol. NMR 6*, 277–293.
67. Johnson, B. A., and Blevins, R. A. (1994) Nmr View: A Computer Program for the Visualization and Analysis of Nmr Data. *J. Biomol. NMR 4*, 603–614.
68. Yang, D. W., and Kay, L. E. (1999) Improved (HN)-H-1-detected triple resonance TROSY-based experiments. *J. Biomol. NMR 13*, 3–10.
69. Nietlispach, D. (2005) Suppression of anti-TROSY lines in a sensitivity enhanced gradient selection TROSY scheme. *J. Biomol. NMR 31*, 161–166.
70. Pervushin, K., Vogeli, B., and Eletsky, A. (2002) Longitudinal H-1 relaxation optimization in TROSY NMR spectroscopy. *J. Am. Chem. Soc. 124*, 12898–12902.
71. Zheng, Y., Giovannelli, J. L., Ho, N. T., Ho, C., and Yang, D. (2004) Side-chain assignments of methyl-containing residues in a uniformly ^{13}C-labeled hemoglobin in the carbonmonoxy form. *J. Biomol. NMR 30*, 423–429.
72. Yang, D., Zheng, Y., Liu, D., and Wyss, D. F. (2004) Sequence-specific assignments of methyl groups in high-molecular weight proteins. *J. Am. Chem. Soc. 126*, 3710–3711.
73. Grzesiek, S., and Bax, A. (1993) The importance of not saturating water in protein NMR. Application to sensitivity enhancement and NOE measurements. *J. Am. Chem. Soc. 115*, 12593–12594.
74. Grzesiek, S., Bax, A., Hu, J. S., Kaufman, J., Palmer, I., Stahl, S. J., Tjandra, N., and Wingfield, P. T. (1997) Refined solution structure and backbone dynamics of HIV-1 Nef. *Protein Sci. 6*, 1248–1263.
75. Piotto, M., Saudek, V., and Sklenar, V. (1992) Gradient-Tailored Excitation for Single-Quantum Nmr-Spectroscopy of Aqueous-Solutions. *J. Biomol. NMR 2*, 661–665.
76. Shaka, A. J., Keeler, J., and Freeman, R. (1983) Evaluation of a New Broad-Band Decoupling Sequence: Waltz-16. *J. Magn. Reson. 53*, 313–340.
77. Shaka, A. J., Barker, P. B., and Freeman, R. (1985) Computer-Optimized Decoupling Scheme for Wideband Applications and Low-Level Operation. *J. Magn. Reson. 64*, 547–552.
78. Marion, D., Ikura, M., Tschudin, R., and Bax, A. (1989) Rapid Recording of 2d Nmr-Spectra without Phase Cycling: Application to the Study of Hydrogen-Exchange in Proteins. *J. Magn. Reson. 85*, 393–399.
79. Cavanagh, J., and Rance, M. (1990) Sensitivity Improvement in Isotropic Mixing (Tocsy) Experiments. *J. Magn. Reson. 88*, 72–85.
80. Palmer, A. G., Cavanagh, J., Wright, P. E., and Rance, M. (1991) Sensitivity Improvement in Proton-Detected 2-Dimensional Heteronuclear Correlation Nmr-Spectroscopy. *J. Magn. Reson. 93*, 151–170.

81. Dominguez, C., Boelens, R., and Bonvin, A. M. J. J. (2003) HADDOCK: A protein-protein docking approach based on biochemical or biophysical information. *J. Am. Chem. Soc. 125*, 1731–1737.
82. Brunger, A. T. (2007) Version 1.2 of the Crystallography and NMR system. *Nat. Protoc. 2*, 2728–2733.
83. Brunger, A. T., Adams, P. D., Clore, G. M., DeLano, W. L., Gros, P., Grosse-Kunstleve, R. W., Jiang, J. S., Kuszewski, J., Nilges, M., Pannu, N. S., Read, R. J., Rice, L. M., Simonson, T., and Warren, G. L. (1998) Crystallography & NMR system: A new software suite for macromolecular structure determination. *Acta Crystallogr. D54*, 905–921.
84. Hubbard, S. J., Eisenmenger, F., and Thornton, J. M. (1994) Modeling Studies of the Change in Conformation Required for Cleavage of Limited Proteolytic Sites. *Protein Sci. 3*, 757–768.
85. Hubbard, S. J., Thornton, J. M., and Campbell, S. F. (1992) Substrate Recognition by Proteinases. *Faraday Discuss.,* 13–23.
86. Krissinel, E., and Henrick, K. (2007) Inference of macromolecular assemblies from crystalline state. *J. Mol. Biol. 372*, 774–797.
87. Sobolev, V., Sorokine, A., Prilusky, J., Abola, E. E., and Edelman, M. (1999) Automated analysis of interatomic contacts in proteins. *Bioinformatics 15*, 327–332.
88. Koradi, R., Billeter, M., and Wuthrich, K. (1996) MOLMOL: A program for display and analysis of macromolecular structures. *J. Mol. Graphics 14* (51−55), 29–32.
89. DeLano, W. L. (2002) Unraveling hot spots in binding interfaces: Progress and challenges. *Curr. Opin. Struct. Biol. 12*, 14–20.
90. Anglister, J. (1990) Use of deuterium labelling in NMR studies of antibody combining site structure. *Q. Rev. Biophys. 23*, 175–203.
91. Anglister, J., Levy, R., and Scherf, T. (1989) Interactions of antibody aromatic residues with a peptide of cholera toxin observed by two-dimensional transferred nuclear Overhauser effect difference spectroscopy. *Biochemistry 28*, 3360–3365.
92. Scherf, T., and Anglister, J. (1993) A T1ρ-filtered two-dimensional transferred NOE spectrum for studying antibody interactions with peptide antigens. *Biophys. J. 64*, 754–761.
93. Levy, R., Assulin, O., Scherf, T., Levitt, M., and Anglister, J. (1989) Probing antibody diversity by 2D NMR: Comparison of amino acid sequences, predicted structures, and observed antibody-antigen interactions in complexes of two antipeptide antibodies. *Biochemistry 28*, 7168–7175.
94. Scherf, T., Hiller, R., and Anglister, J. (1995) NMR observation of interactions in the combining site region of an antibody using a spin-labeled peptide antigen and NOESY difference spectroscopy. *FASEB J. 9*, 120–126.
95. Anglister, J., and Naider, F. (1991) Nuclear magnetic resonance for studying peptide-antibody complexes by transferred nuclear Overhauser effect difference spectroscopy. *Methods Enzymol. 203*, 228–241.
96. Zvi, A., Feigelson, D. J., Hayek, Y., and Anglister, J. (1997) Conformation of the principal neutralizing determinant of human immunodeficiency virus type 1 in complex with an anti-gp120 virus neutralizing antibody studied by two-dimensional nuclear magnetic resonance difference spectroscopy. *Biochemistry 36*, 8619–8627.
97. Cierpicki, T., and Bushweller, J. H. (2004) Charged gels as orienting media for measurement of residual dipolar couplings in soluble and integral membrane proteins. *J. Am. Chem. Soc. 126*, 16259–16266.
98. Akabayov, S. R. (2007) in Structural Biology, pp 141, Weizmann Institute of Science, Rehovot, Israel.
99. Uze, G., Schreiber, G., Piehler, J., and Pellegrini, S. (2007) The receptor of the type I interferon family. *Curr. Top. Microbiol. Immunol. 316*, 71–95.
100. Pearce, K. H., Jr., Ultsch, M. H., Kelley, R. F., de Vos, A. M., and Wells, J. A. (1996) Structural and mutational analysis of affinity-inert contact residues at the growth hormone-receptor interface. *Biochemistry 35*, 10300–10307.
101. Akabayov, S. R., Biron, Z., Lamken, P., Piehler, J., and Anglister, J. (2010) NMR Mapping of the IFNAR1-EC binding site on IFNalpha2 reveals allosteric changes in the IFNAR2-EC binding site. *Biochemistry 49*, 687–695.
102. Bhattacharya, A., Tejero, R., and Montelione, G. T. (2007) Evaluating protein structures determined by structural genomics consortia. *Proteins 66*, 778–795.